

MP3: Movement Primitive-Based (Re-)Planning Policy

Fabian Otto*

FABIAN.OTTO@BOSCH.COM

*Bosch Center for Artificial Intelligence
University of Tübingen, Tübingen, 72076, Germany*

Hongyi Zhou*

HONGYI.ZHOU@KIT.EDU

*Intuitive Robots Lab
Karlsruhe Institute of Technology, Karlsruhe, 76131, Germany*

Onur Celik

CELIK@KIT.EDU

*Autonomous Learning Robots Lab
Karlsruhe Institute of Technology, Karlsruhe, 76131, Germany*

Ge Li

GE.LI@KIT.EDU

*Autonomous Learning Robots Lab
Karlsruhe Institute of Technology, Karlsruhe, 76131, Germany*

Rudolf Lioutikov

LIOUTIKOV@KIT.EDU

*Intuitive Robots Lab
Karlsruhe Institute of Technology, Karlsruhe, 76131, Germany*

Gerhard Neumann

GERHARD.NEUMANN@KIT.EDU

*Autonomous Learning Robots Lab
Karlsruhe Institute of Technology, Karlsruhe, 76131, Germany*

Editor: My editor

Abstract

We introduce a novel deep reinforcement learning (RL) approach called Movement Primitive-based Planning Policy (MP3). By integrating movement primitives (MPs) into the deep RL framework, MP3 enables the generation of smooth trajectories throughout the whole learning process while effectively learning from sparse and non-Markovian rewards. Additionally, MP3 maintains the capability to adapt to changes in the environment during execution. Although many early successes in robot RL have been achieved by combining RL with MPs, these approaches are often limited to learning single stroke-based motions, lacking the ability to adapt to task variations or adjust motions during execution. Building upon our previous work, which introduced an episode-based RL method for the non-linear adaptation of MP parameters to different task variations, this paper extends the approach to incorporating replanning strategies. This allows adaptation of the MP parameters throughout motion execution, addressing the lack of online motion adaptation in stochastic domains requiring feedback. We compared our approach against state-of-the-art deep RL and RL with MPs methods. The results demonstrated improved performance in sophisticated, sparse reward settings and in domains requiring replanning. The video demonstration can be accessed at https://intuitive-robots.github.io/mp3_website/.

Keywords: Movement primitives, deep reinforcement learning, trust regions, robot learning, sparse and non-Markovian rewards

*. Equal contribution: order determined by alphabet.

1 Introduction

Movement primitives (MPs) are a powerful and versatile method for representing robot trajectories with a concise set of parameters. This makes MPs an easy-to-use and efficient tool for reinforcement learning (RL) tasks. By directly exploring the space of desired trajectories, MPs simplify the exploration process and produce smooth, “robot-friendly” motions. As a result, RL with MPs (MPRL) has been responsible for many of the early successes in robot RL, with notable applications in Table-Tennis (Mülling et al., 2013; Gomez-Gonzalez et al., 2016), Ball-In-A-Cup (Kormushev et al., 2010), and Pan-Cake-Flipping (Kormushev et al., 2013). However, these algorithms were previously limited to simple setups and could only learn single stroke-based open-loop motions. Consequently, these motions were difficult to adapt to task variations or during motion execution. With increasing computation power, the field of deep RL rose. These methods can learn complex closed-loop sensorimotor policies, which is the reason why this research field dominated recent years. In this paper, we extend our work given in Otto et al. (2021) and Otto et al. (2022) to address the shortcomings of previous RL with MPs approaches and propose a new method that integrates MPs into a deep RL pipeline. Our method allows for non-linear adaptation and replanning during execution of the MP, while still maintaining the beneficial exploration properties of the MP framework in the context of RL.

Traditional deep RL methods use a step-based policy, where at each time step the policy explores in the atomic action space. During interaction with the environment, the agent collects state, action, and reward data points at each time step, which are used to update the policy. Although using every atomic action generates a vast amount of data-points for the policy update, it also complicates exploration due to the typical random walk behavior and introduces a lot of noise in the policy evaluation process (see Figure 2). Therefore, these methods often rely on informative reward signals throughout the interaction sequence, making them less effective in sparse or temporally sparse settings where feedback from the environment is delayed. Moreover, step-based exploration can result in slower convergence and jerky, potentially dangerous behavior for the agent.

In contrast, MPRL is typically based on episode-based RL (ERL) (Deisenroth et al., 2013; Abdolmaleki et al., 2015; Daniel et al., 2012; Otto et al., 2022). ERL methods learn to parameterize a desired trajectory used for a controller based on a task description known as the context, which remains fixed throughout the entire episode. For example, in a table tennis scenario, the context is given by the target position where the robot has to return the ball. These methods explore the trajectory space, meaning that a parameter is sampled given the context only once at the beginning of the episode and executed without resampling. This exploration strategy results in time-correlated exploration, smooth behaviors, and improved performance in sparse or non-Markovian reward settings (Otto et al., 2022). Yet, only one data point is generated per executed trajectory, as these algorithms collect only one context-parameter pair per episode. This data collection procedure limits sample efficiency. In our recent work (Otto et al., 2022), we integrated ERL with MPs into a deep policy gradient algorithm that is based on trust region projection layer (TRPL) (Otto et al., 2021). While this algorithm can non-linearly adapt the parameters of the MP to the given context and achieve high-quality policies for complex robotic tasks, it is inherently constrained to generating open-loop trajectories that cannot be adapted or adjusted during execution.

This paper is an extension of Otto et al. (2022), where we also add learning non-linear re-planning policies instead of just the initial adaptation of the MP to the context, combining the benefits of ERL with MPs and step-based RL (SRL) methods. We still explore in the trajectory space, yet, the agent is now able to change the desired trajectory during an episode, enabling it to adapt its behavior to unpredictable changes in the environment. In the original paper (Otto et al., 2022), probabilistic movement primitives (ProMPs) (Paraschos et al., 2013) were used as the MP representation. However, ProMPs are unable to generate smooth trajectories if the MP parameters are changed during motion execution. As a result, ProMPs are not suitable for learning replanning policies. In contrast, in this paper, we employ the recently introduced probabilistic dynamic movement primitives (ProDMPs) (Li et al., 2022) to address the limitations of commonly used MPs (Schaal et al., 2005; Schaal, 2006; Paraschos et al., 2013). ProDMP constitute a reformulation of the popular dynamic movement primitive (DMP) (Schaal, 2006; Ijspeert et al., 2013) framework which is better suited to be integrated into a neural network architecture as it does not require expensive numerical integration. Additionally, ProDMP can use any initial state as the initial condition, allowing for the generation of smooth desired trajectories even when applying replanning. Our policies are parameterized with neural networks and efficiently trained using TRPL (Otto et al., 2022), which has demonstrated significantly improved stability and quality of the learned policy in comparison to other policy gradient methods, such as proximal policy optimization (PPO) (Schulman et al., 2017). We demonstrate the effectiveness of our method by presenting various complex simulated robotic tasks, such as robot table tennis, beer-pong, a complex box-pushing task, and large-scale manipulation tasks on Meta-World (Yu et al., 2019). We compare our approach to state-of-the-art SRL and ERL methods and illustrate improved performance in sophisticated, sparse reward settings and settings that require replanning.

2 Background and Related Work

(Step-Based) Reinforcement Learning. In SRL, direct interactions with the environment involve using raw action inputs based on the current state. These predicted actions typically correspond to positions, velocities, or torques in robotic tasks. They represent the specific control signals that are applied to the robot’s actuators, influencing its movements and behavior. On-policy RL refers to the methods that use the same policy for exploration and update. Here, policy gradient methods (Sutton et al., 1999; Schulman et al., 2015, 2017) are often used as they are straightforward to implement and yield high-quality policies. These methods typically apply some form of trust region to stabilize the on-policy update due to the large variance of the gradients. PPO (Schulman et al., 2017) is one of the most commonly used methods. It introduced a clipping heuristic to the policy gradient objective as an approximation of the trust region. It has shown robust and efficient performance even in large-scale problems, such as OpenAI Five (Berner et al., 2019) and GPT-4 (OpenAI, 2023), but can depend heavily on the implementation details (Engstrom et al., 2020) and uses ad-hoc heuristics that do not work well for complex exploration problems (Otto et al., 2021, 2022). In contrast to the above methods, soft actor critic (SAC) and twin-delayed deep deterministic policy gradient (TD3) are off-policy methods. They tend to exhibit higher sample efficiency, but are often computationally more expensive. Addi-

tionally, they may introduce a higher bias in the policy update due to the reliance on the critic network to evaluate the actions. We choose to compare our algorithm against PPO and SAC as these are currently the most popular on-policy and off-policy RL algorithms.

Trust Region Projection Layers. Enforcing trust regions is an established technique to ensure the stability and convergence of policy gradient methods. While existing efficient methods, such as PPO, use surrogate cost functions as approximations of trust regions, they cannot enforce the trust region exactly. This limitation was addressed in trust region projection layers (TRPLs) (Otto et al., 2021), which presents a mathematically sound and scalable approach to enforce exact trust regions in deep SRL. The algorithm efficiently enforces a trust region for each input state of the policy using differentiable convex optimization layers (Agrawal et al., 2019), providing more stability and control during training and at the same time reduce the dependency on implementation choices (Engstrom et al., 2020).

The layer receives the standard output of a Gaussian policy, which includes the mean $\boldsymbol{\mu}$ and covariance $\boldsymbol{\Sigma}$, and applies a projection operation to enforce a trust region when the mean and covariance exceed their respective bounds. This projection is performed individually for each input state. The resulting Gaussian policy distribution, characterized by the adjusted parameters $\tilde{\boldsymbol{\mu}}$ and $\tilde{\boldsymbol{\Sigma}}$, is then used for subsequent computations, e.g. sampling and loss computation. Formally, the layer solves the following two optimization problems for each state \mathbf{s}

$$\begin{aligned} \arg \min_{\tilde{\boldsymbol{\mu}}_s} d_{\text{mean}}(\tilde{\boldsymbol{\mu}}_s, \boldsymbol{\mu}(\mathbf{s})), \quad \text{s.t.} \quad d_{\text{mean}}(\tilde{\boldsymbol{\mu}}_s, \boldsymbol{\mu}_{\text{old}}(\mathbf{s})) \leq \epsilon_{\boldsymbol{\mu}}, \quad \text{and} \\ \arg \min_{\tilde{\boldsymbol{\Sigma}}_s} d_{\text{cov}}(\tilde{\boldsymbol{\Sigma}}_s, \boldsymbol{\Sigma}(\mathbf{s})), \quad \text{s.t.} \quad d_{\text{cov}}(\tilde{\boldsymbol{\Sigma}}_s, \boldsymbol{\Sigma}_{\text{old}}(\mathbf{s})) \leq \epsilon_{\boldsymbol{\Sigma}}, \end{aligned}$$

where $\tilde{\boldsymbol{\mu}}_s$ and $\tilde{\boldsymbol{\Sigma}}_s$ are the optimization variables for input state \mathbf{s} and $\epsilon_{\boldsymbol{\mu}}$ and $\epsilon_{\boldsymbol{\Sigma}}$ are the trust region bounds for mean and covariance, respectively. We measure the similarity between means and covariances using d_{mean} and d_{cov} , which are decomposable similarity measures. Although Otto et al. (2021) proposed three such measures (KL, Wasserstein, and Frobenius), we only use the decomposed KL-divergence in this work as it showed the most promising performance in the original work. This measure can be made fully differentiable by following the method described in Otto et al. (2021) and is explained in more detail in Appendix B.

Episode-based Reinforcement Learning. In the framework of contextual episode-based policy search (Deisenroth et al., 2013; Daniel et al., 2012), RL is treated as a black-box optimization problem. The goal is to maximize the expected return $R(\mathbf{w}, \mathbf{c})$ by optimizing a contextual search distribution $\pi(\mathbf{w}|\mathbf{c})$ over the controller parameters \mathbf{w} . Here, the context vector \mathbf{c} characterizes the given task, for instance, given by a goal location or the location of an object, and the controller is typically given by a motion primitive. The objective can be expressed as

$$\arg \max_{\pi(\mathbf{w}|\mathbf{c})} \mathbb{E}_{p(\mathbf{c})} [\mathbb{E}_{\pi(\mathbf{w}|\mathbf{c})} [R(\mathbf{w}, \mathbf{c})]],$$

where $p(\mathbf{c})$ denotes the context distribution given by the task. The return function $R(\mathbf{w}, \mathbf{c})$ is not subject to any structural assumptions, and it can be any non-Markovian function of

the resulting trajectory due to the black-box nature of the problem. Most ERL algorithms are focused on the non-contextual setting, where different optimization techniques have been used, such as policy gradients (Sehnke et al., 2010), natural gradients (Wierstra et al., 2014), stochastic search strategies (Hansen and Ostermeier, 2001; Mannor et al., 2003; Abdolmaleki et al., 2019), or trust-region optimization techniques (Abdolmaleki et al., 2015; Daniel et al., 2012; Tangkaratt et al., 2017). Early methods that incorporate context adaptation (Tangkaratt et al., 2017; Abdolmaleki et al., 2019) only consider a linear mapping from context to parameter space, which is a major limitation on the performance of these approaches. In contrast, we consider highly nonlinear context-parameter relationships using neural networks.

Evolutionary Strategies. Recent work from the domain of evolutionary strategies (Mania et al., 2018; Salimans et al., 2017; Chrabaszcz et al., 2018) have also proposed full gradient-free black-box approaches as an alternative to gradient- and step-based methods for finding optimal neural network parameters. These approaches treat learning the neural network policy parameters (several thousand parameters) as the black-box optimization problem as opposed to learning movement primitive parameters (20-50 parameters). While these methods can be competitive for black-box optimization of neural networks, they typically do not consider contextual setups where different parameters have to be chosen for different contexts, as it is common for movement primitives. In the contextual case, the performance of the rollout depends on both the parameter vector and the context (for instance, the goal), introducing additional noise to the evaluation if the method is context ignorant. For example, a good neural network parametrization can still yield a poor performance because it has been evaluated in a difficult context. The above approaches are completely ignorant to the context and, therefore, are not competitive for complex contextual scenarios as shown in our experiments.

In contrast, we do not engage in black-box optimization at the level of a global neural network control policy, which would involve thousands of parameters. Rather, we focus on local control parameters of movement primitives or similar controllers, which only have 10 – 50 dimensions. We still use neural network policy with a substantial number of parameters to predict these local control parameters based on the context. Instead of optimizing these neural network parameters in a black-box manner, we update them via policy gradient, which uses both the context information as well as the policy derivatives.

Reinforcement Learning with Movement Primitives. While most works of MPRL concentrate on learning a single MP parameter vector for a single task configuration (Abdolmaleki et al., 2015; Kober and Peters, 2008; Stulp and Sigaud, 2012a,b), some methods allow linear adaptation of the MP’s parameter vector to the context (Daniel et al., 2012; Kupcsik et al., 2017; Celik et al., 2022). In addition, a few RL approaches leverage non-linear policies combined with predefined action primitives, such as pushing or grasping motions (Dalal et al., 2021; Zenkri et al., 2022). One approach that directly uses MPs and deep networks in a SRL setting is neural dynamic policies (NDP) (Bahl et al., 2020). NDP aims to embed the structure of DMPs into deep policies by reparameterizing action spaces via second-order differential equations. This can be seen as an intersection between step-based and episode-based methods by learning sub-trajectories via DMPs spanning multiple timesteps. While their approach enables effective replanning, unlike our approach, their

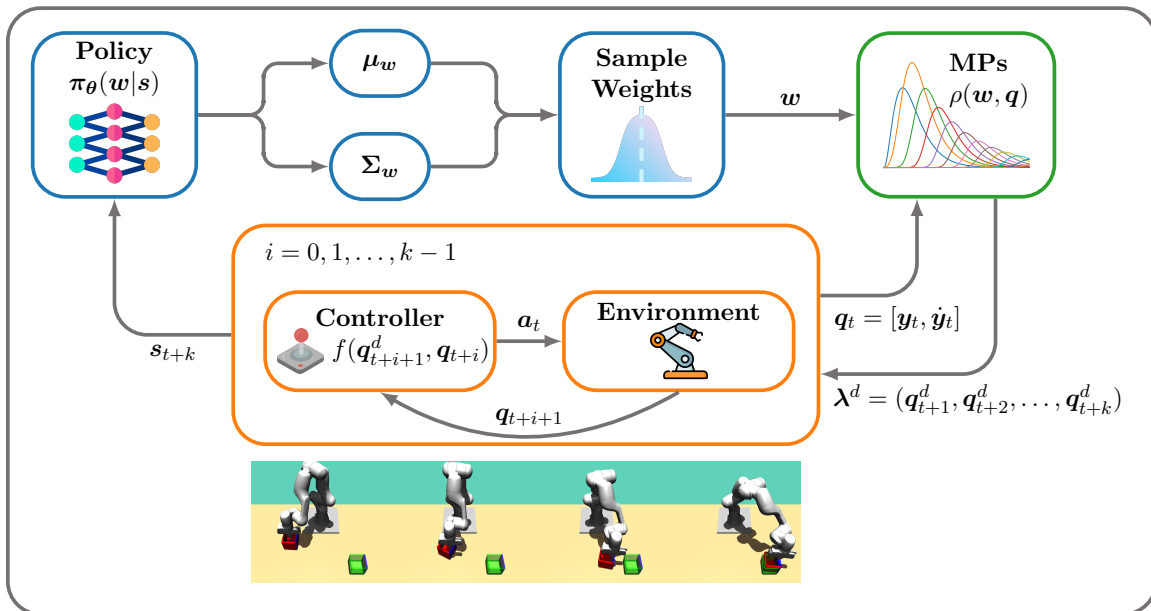


Figure 1: This figure provides an overview of the proposed framework that combines deep RL with MPs. Instead of generating a raw action directly, the policy generates a set of weights that parameterizes a MP. The MP predicts a desired trajectory given the weights and initial conditions, which is then converted to raw actions using a tracking controller.

main exploration still takes place at the action level rather than at the trajectory level, similar to standard step-based approaches, which neglects the main benefit of using MPs in an RL context. Moreover, using DMPs requires several numerical integration steps that also need to be differentiated, making it computationally expensive. In our experiments, NDP performs poorly, which contradicts the original paper. This is mainly because we use a different measure for sample efficiency. In contrast to the original paper where only the number of samples used in policy updates are counted, we report the total number of environment interactions as we believe this choice provides a more straightforward insight into the training cost associated with each method.

3 Deep Reinforcement Learning with Movement Primitives

In this work, we present a framework to effectively combine MPs with deep RL methods. This framework consists of three major components (see Figure 1):

- One RL policy which takes the environment observation as input and outputs an MP weight vector that is used for multiple time steps.
- One MP model which uses the weight vector as input to generate a desired trajectory.
- One low-level controller which converts the desired trajectory into raw actions and interacts with the environment.

This approach is simple but highly versatile. Theoretically, any policy search algorithm applicable to continuous action spaces can be used here. However, it is worth noting that the dimensionality of the weight space of the MP is usually larger than the raw action space. Therefore, the policy search algorithm used must be able to explore high-dimensional spaces efficiently. Furthermore, MPs can be replaced by any parameterized trajectory generator, as long as the desired trajectory can be uniquely determined by a weight vector. We specifically chose MPs in this work because they are capable of generating smooth trajectories and allowing effective replanning. In addition, the planning horizon (length of the generated trajectory before a new weight vector is chosen) can vary from a single step to the entire episode. Two special cases correspond to two common RL paradigms: (i) When the planning horizon is equal to one, our framework is similar to an SRL algorithm (although with a higher dimensional action space). (ii) When it is equal to the episode length, the framework corresponds to an ERL algorithm.

3.1 Movement Primitives

MPs are a widely used tool for motion representation and generation in robotics. They are used as building blocks for movements, allowing for the modulation of motion behavior and the creation of more complex movements through combination or concatenation. With their concise parameterization and flexibility, MPs have become a popular choice in imitation learning (Maeda et al., 2014; Gomez-Gonzalez et al., 2016; Pahič et al., 2020; Li et al., 2022; Rozo and Dave, 2022) and RL (Celik et al., 2022; Li et al., 2017). In this work, we focus on using trajectory-based movement representations, as discussed in previous work for RL (Schaal, 2006; Ijspeert et al., 2013; Paraschos et al., 2013; Li et al., 2022). Given a parameter vector, these representations generate desired trajectories for the agent to follow, and the goal is often to optimize the weight vector or its distribution to improve the resulting movements.

Probabilistic Movement Primitives (ProMPs). ProMPs (Paraschos et al., 2013) generate the trajectory λ by a linear basis function model

$$y(t) = \Phi^\top(t)\mathbf{w}, \quad \lambda = [y_t]_{t=0:T} = \Phi_{0:T}^\top \mathbf{w},$$

where \mathbf{w} is the time-independent weight vector, $y(t)$ is the trajectory position at time step t and Φ are pre-defined time-dependent basis functions, for instance, normalized RBF basis. Due to the simplicity of the linear basis function representation, ProMPs allow for fast trajectory computation and enable modeling the trajectory’s statistics from the weight vector’s distribution. Such statistics often include temporal correlations of the trajectories and the motion correlations across different degree of freedom (DoF). One of the key limitations of ProMPs as a representation method is their lack of smoothness in trajectory replanning and concatenation, which means when choosing a \mathbf{w} , there is no guarantee that the trajectory will start from the desired initial conditions at the current time step. This lack of smoothness and inability to adjust the trajectory’s start state poses limitations in the practical application of ProMPs, especially in situations where the weight vector needs to be updated throughout motion execution due to unpredictable changes in the environment.

Dynamic Movement Primitives (DMPs). DMPs (Schaal, 2006; Ijspeert et al., 2013) form a trajectory by integrating a dynamic system, providing smooth replanning of both

position and velocity (Brandherm et al., 2019; Ginesi et al., 2019; Lee et al., 2020). However, this smoothness comes at a computational cost, as DMPs require online numerical integration to compute a trajectory. When using DMPs in neural networks, the forward and backward pass of the networks become coupled with this numerical integration (Bahl et al., 2020; Pahič et al., 2018, 2020), leading to complex and slow models.

Probabilistic Dynamic Movement Primitives (ProDMPs). To combine the advantages and address the limitations of ProMPs and DMPs, Li et al. (2022) recently proposed ProDMPs by solving the DMP’s underlying ordinary differential equation (ODE). The expensive online numerical integration of DMPs is replaced by position and velocity basis functions, which can be computed offline and shared by all trajectories. This results in a representation of trajectory position and velocity that is similar to that of ProMPs, expressed as:

$$y(t) = c_1 y_1(t) + c_2 y_2(t) + \Phi(t)^\top \mathbf{w}_g, \quad \dot{y}(t) = c_1 \dot{y}_1(t) + c_2 \dot{y}_2(t) + \dot{\Phi}(t)^\top \mathbf{w}_g,$$

where y_1 and y_2 denote the two linearly independent complementary functions of the governing ODE of DMPs. Their corresponding derivatives w.r.t time are \dot{y}_1, \dot{y}_2 . The coefficients c_1 and c_2 , which are shared by both position and velocity representations, are determined by solving an initial condition problem of the ODE. The position and velocity basis functions, denoted by Φ and $\dot{\Phi}$ respectively, can be computed only once offline and later used as constant functions. The vector \mathbf{w}_g in both equations concatenates the DMP’s original weights \mathbf{w} and goal attractor g into one vector. To simplify our notation, we will refer to all learned parameters collectively as \mathbf{w} from this point forward. A brief derivation of these equations is provided in Appendix A, for the further details, we refer the reader to the original paper (Li et al., 2022).

Theoretically, both DMP and ProDMP can be used in domains requiring online replanning. In this work, we specifically use the ProDMPs model as our trajectory generator because it ensures smooth replanning with low computational cost.

3.2 Reinforcement Learning Objective with Movement Primitives

While traditional SRL methods rely on single raw actions $\mathbf{a}_t \in \mathcal{A}$ per time step, we train a policy to select a weights vector $\mathbf{w}_t \in \mathcal{W}$ in MP’s parameter space \mathcal{W} . The weights vector is then translated to a desired trajectory of the proprioceptive states $\boldsymbol{\lambda}^d = (\mathbf{q}_{t+1}^d, \mathbf{q}_{t+2}^d, \dots, \mathbf{q}_{t+k}^d)$, where $q_t^d = [\mathbf{y}_t^d, \dot{\mathbf{y}}_t^d]$ consists of desired position \mathbf{y}_t^d and desired velocity $\dot{\mathbf{y}}_t^d$ at time step t , and k denotes the planning horizon. Given the desired trajectory and the measured proprioceptive state, a tracking controller $f(q_t^d, q_t)$ decides the action at each step, resulting in a trajectory in the raw action space $(\mathbf{a}_{t+1}, \mathbf{a}_{t+2}, \dots, \mathbf{a}_{t+k}) \in \mathcal{A}$. In contrast to the step-wise sample $(\mathbf{s}_t, \mathbf{a}_t, R_t)$ used in SRL, we use temporarily-abstracted samples of the form $(\mathbf{s}_t, \mathbf{w}_t, R_t^k)$. The reward $R_t^k = R_{t:t+k-1}$ of each trajectory segment is defined as the cumulative reward over all the segment’s time steps t to $t+k-1$

$$R_t^k(\mathbf{s}_t, \mathbf{w}_t) = \sum_{i=0}^{k-1} \gamma^i r(\mathbf{s}_{t+i}, \mathbf{a}_{t+i}), \tag{1}$$

where \mathbf{a}_t and \mathbf{s}_t are the executed actions and observed states following the desired trajectory and tracked by the controller. While our approach supports different k for each segment,

we only consider planning segments with equal length in this work. We can compute the episode return by taking the cumulative discounted sum of the segment rewards. Using the notation from above, we can express this as

$$G_t^k = \sum_{i=0}^{\lceil T/k-1 \rceil} \gamma^{ik} R_{t+ki}^k(\mathbf{w}_{t+ki}, \mathbf{s}_{t+ki}), \quad (2)$$

where $\gamma \in (0, 1]$ is the discount factor. It is worth noting that there are two special cases to consider. In the black-box setting, in other words, when the MP parameters are chosen only at the beginning of the episode, then $k = T$ and the segment reward equals the episode return

$$R_0^{T-1} = \sum_{t=0}^{T-1} \gamma^t r(a_t, s_t). \quad (3)$$

The second special case is step-based RL. That is, we choose a new parameter vector at every time step and $k = 1$. In this case, segment reward is equivalent to step reward

$$R_t^1 = r(a_t, s_t). \quad (4)$$

This gives the insight that we can alter between SRL and ERL by choosing different planning horizons k .

3.3 Policy-gradients for MP weight-selection policies

With these rewards, we can now also define matching value and advantage functions

$$V^\pi(\mathbf{s}) = \mathbb{E} \left[G_t^k | \mathbf{s}_t = \mathbf{s}; \pi_\theta \right] \quad A^\pi(\mathbf{s}, \mathbf{w}) = \mathbb{E} \left[G_t^k | \mathbf{s}_t = \mathbf{s}, \mathbf{w}_t = \mathbf{w}; \pi_\theta \right] - V^\pi(\mathbf{s}). \quad (5)$$

Following the step-based policy gradient (Williams, 1992; Schulman et al., 2015), we optimize the advantage function using the likelihood ratio gradient and an importance sampling estimator. The resulting objective

$$\hat{J}(\pi_\theta, \pi_{\theta_{\text{old}}}) = \mathbb{E}_{(\mathbf{s}, \mathbf{w}) \sim p(\mathbf{s}), \pi_{\theta_{\text{old}}}} \left[\frac{\pi_\theta(\mathbf{w} | \mathbf{s})}{\pi_{\theta_{\text{old}}}(\mathbf{w} | \mathbf{s})} A^{\pi_{\theta_{\text{old}}}}(\mathbf{s}, \mathbf{w}) \right], \quad (6)$$

is maximized w.r.t θ , with $\pi_{\theta_{\text{old}}}$ being the old behavior policy used for sampling. We can further make use of a learned state-value function $V_\phi(\mathbf{s}) \approx V^\pi(\mathbf{s})$ for the advantage estimator, which is approximated by optimizing

$$\arg \min_{\phi} \mathbb{E}_{(\mathbf{s}, \mathbf{w}) \sim p(\mathbf{s}), \pi_{\theta_{\text{old}}}} \left[(V_\phi(\mathbf{s}) - G_t^k)^2 \right]. \quad (7)$$

This formulation also enables the use of advantage estimation methods, such as general advantage estimation (Schulman et al., 2016). During the update of the policy, neither the MP $\rho(\mathbf{w}, \mathbf{q})$ nor the controller $f(\mathbf{q}_{t+1}^d, \mathbf{q}_t)$ are needed, i.e., our approach would work with any form of parametrizable controller.

3.4 Choice of the Deep Reinforcement Learning Algorithm

Most deep RL methods can theoretically be used to train policies in the weight space of MPs. Yet, training in this space requires learning policies with a higher degree of precision compared to the step-based case as the selected action is active for more time steps with no opportunity for correction during the trajectory segment. To address this issue, we chose TRPL as it has been shown to be more stable and accurate than other RL methods (Otto et al., 2021). TRPL implements exact trust regions for policy updates and enforces them per state, while most other deep RL methods (Schulman et al., 2015, 2017; Akrouer et al., 2019) only provide approximate trust region updates that are enforced for the average policy change across all states.

3.5 Choice of the Planning Horizon

Our method harnesses the merits of two common RL paradigms: step-based RL (SRL) and episode-based RL (ERL). The agent’s behavior can seamlessly switch between the two paradigms according to the planning horizon k . As discussed previously, there are two special cases when selecting the planning horizon.

Black-Box Setting. The first special case arises when the planning horizon is equal to the episode length, that is, $k = T$. In this case, the agent generates only one desired trajectory for the entire episode, similar to an open-loop motion planner. We refer to this setting as MP3-Black Box (MP3-BB) in the following discussion, since it treats reinforcement learning as a black-box optimization problem. MP3-BB does not assume the existence of a step reward, but instead evaluates the performance of the entire trajectory as a whole. The black-box nature facilitates dealing with sparse and non-Markovian rewards, leading to a more intuitive reward design. Another advantage is state abstraction. The MP3-BB agent does not need any intermediate state information about the task execution that varies during the execution process (such as joints position/velocity, etc.), but focuses only on the critical information that defines the essence of the tasks (for example goals, obstacles, etc.), this is also referred to as context. However, MP3-BB presents some challenges. Although the reduction of the observation dimension to the context space results in a modest impact on sample efficiency, the high cost of a single sample makes it less sample-efficient. Moreover, its black-box nature limits its applicability in dynamic environments, where the agent must adapt to environmental changes during execution.

Step-Based Setting. At the opposite end of the planning horizon spectrum is the case where $k = 1$. Here, the agent only executes the desired trajectory for one step, after which it generates a new plan, repeating this loop throughout the episode similar to the SRL setting. However, using MPs as a trajectory generator instead of raw actions has two essential differences. Firstly, the use of MPs guarantees second-order smoothness (position and velocity), resulting in a more consistent and smooth behavior during exploration and evaluation (see Figure 2). Secondly, the number of MP basis functions is a hyperparameter that allows for scaling the dimension of the action space from the size of raw actions to arbitrary dimensions, enriching the model’s design choices but also increasing the complexity. Although increasing the dimensionality of the action space may seem to increase exploration difficulty, it can still benefit from the smooth trajectories generated by MPs. Nonetheless, we did not

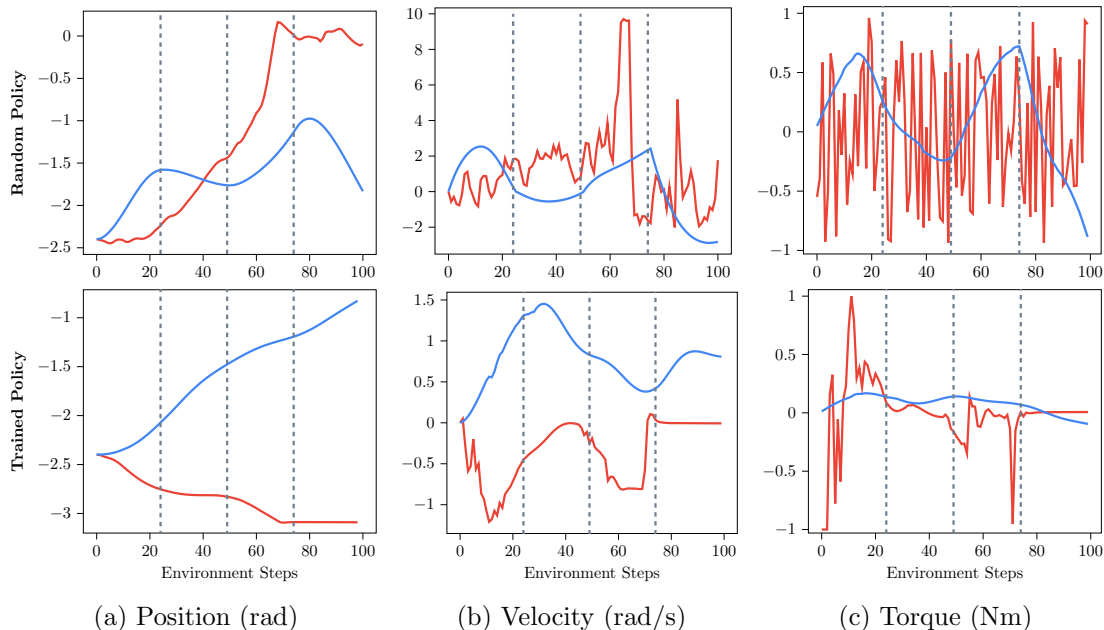


Figure 2: This figure presents a comparison between step-level exploration (red) and the proposed trajectory-level exploration using MPs (blue). We generated rollouts in box-pushing environments where the raw action space is joint torques. For the MP setting, we used ProDMP and performed replanning every 25 steps. The trajectories of the 3rd joint are plotted. In the top row, we randomly sampled rollouts from untrained policies to demonstrate the initial exploration. In the bottom row, we evaluated two policies trained with PPO (red) and MP3 (blue) respectively, using 40M environment interactions. The results show that MP3 enables smooth trajectory generation at both exploration and evaluation processes.

observe significant improvements using this setting over the standard SRL setting, and our discussion only aims to highlight the flexibility of the proposed method.

Re-planning with MPs. The more general case falls somewhere between the two extremes of SRL and ERL. In this approach, the agent generates a new desired trajectory after executing the current trajectory for a predefined number of steps ($1 < k < T$). This method leverages the strengths of both SRL and ERL while addressing some of their shortcomings:

1. In SRL, stochastic raw action selection often results in jerky random walk behavior that does not fully explore the trajectory space of the agent. In contrast, our approach explores the weight space of MPs, leveraging the MP’s smoothness guarantees for more consistent and effective exploration (see Figure 2).
2. Stochastic raw action selection in SRL also results in noisy returns (see Figure 2), translating to high variance in the policy gradient estimation. The smaller number of exploration steps in the re-planning setting yields less variance in gradient estimation, leading to a more stable policy update.

3. Trajectory-level exploration encapsulates the temporal abstraction within each trajectory segment, reducing the number of decisions to make for each episode and improving the agent’s ability to handle the sparsity in the reward function.
4. The policies trained by SRL often struggled to generate smooth trajectories (see Figure 2) due to the lack of continuity between consecutive steps. In contrast, policies trained with our approach are able to generate smooth trajectories in both the exploration and evaluation processes.
5. The ERL agent only makes decisions at the beginning of each episode and treats each episode as a black-box, thus can deal with the temporal sparsity and non-Markovian property in rewards. However, the black-box perspective also limits their ability to address observation noises and dynamics in the environment, as a result, ERL agents cannot adapt their plan according to the changes in the environment during execution, which makes them less flexible and robust compared to SRLs. Our approach addresses this shortcoming by incorporating periodic re-planning during online execution.

Many SRL algorithms use a similar design called *frame-skipping*, which can help with the partial observability of some Atari games (Braylan et al., 2015). However, frame-skipping just repeats the same action for the “skipped” frames, limiting the trajectory’s expressive capacity. In contrast, planning with MP can “skip” more frames without compromising expressiveness.

3.6 Adapting to Different Reward Settings

The proposed algorithm offers a significant advantage in the flexibility to adapt to different reward signal designs. By considering the information available at each step, the rewards can be classified into three distinct categories.

Dense Rewards. Dense rewards provide task-related feedback signals at each time step. For example, in a reacher task where the objective is to reach a desired point with the end-effector, a common task-related feedback could be the distance between the end-effector and the desired point. Well-shaped dense rewards are crucial for the success of most SRL algorithms. However, designing efficient dense rewards can already be challenging for tasks where evaluating the quality of the action step-wise is difficult, such as in beerpong and table tennis.

Sparse Rewards. Sparse rewards provide task-related feedback only when specified conditions are satisfied. These conditions can be either temporal-related (for instance, providing reward only at episode end) or task-related metrics (for instance, providing reward only when end-effector is close enough to the desired point). Our approach is less affected by the temporal sparse setting because we use highly temporal-abstracted samples in policy updates. In contrast to dense reward signals, sparse rewards are usually more intuitive to design and more suitable for the task where task completion at a specific time point (for instance, the episode end) is desired. Take the aforementioned reacher task as an example, dense reward based on distance error at every step implicitly encourages the agent to reach the desired point as fast as possible, leading to policies with large acceleration and

overshooting. This is undesirable if we only want to reach the target at the end. Temporal sparse rewards address this issue by rewarding the agent based on the final state.

Non-Markovian Rewards. Non-Markovian rewards provide task-related feedback without adhering to the Markovian condition, which means the reward signal is not fully determined by the current state-action pair but also incorporates the past states and actions. The non-Markovian property exists widely in RL tasks. For instance, in playing table tennis, once the ball is hit, the agent’s actions no longer influence the trajectory of the ball. Therefore, the reward is not conditioned solely on the action at that time step but also on the actions preceding the hit. This setting is extremely challenging for SRL algorithms as their policy updates rely on the Markovian assumption. Our approach with the black-box setting can leverage non-Markovian rewards effectively by treating the entire episode trajectory as a single sample.

4 Experimental Results

For our evaluation, we begin by demonstrating the effectiveness of our method in handling sparse rewards, improving precision, and energy efficiency without replanning, that is, in the black-box setting with $k = T$. We investigate challenging control problems that are typically difficult to solve in the standard step-based setting. Next, we conduct a large-scale study on all 50 Meta-World tasks (Yu et al., 2019) to showcase our competitive performance on various robot manipulation tasks that come with highly shaped dense rewards with and without replanning. Finally, we evaluate our method with replanning for several tasks with changing goals or high uncertainties and perform a thorough ablation study. We compare our methods, which we call MP3 and MP3-BB for the replanning and black-box cases respectively, against several other step-based methods, including PPO (Schulman et al., 2017), TRPL (Otto et al., 2021), SAC (Haarnoja et al., 2018), and NDP (Bahl et al., 2020), as well as a deep evolution strategies (ES) (Salimans et al., 2017), the linear adaption method contextual model-based relative entropy stochastic search (CMORE) with ProMPs (Tangkaratt et al., 2017) as well as MP3-PPO (MP3-PPO) and MP3-BB-PPO (MP3-BB-PPO), which are equivalent to MP3 and MP3-BB but trained with PPO instead of TRPL. For the ERL methods (MP3-BB and MP3-BB-PPO), we leverage ProMPs for motion generation and for the replanning versions (MP3 and MP3-PPO), we use ProDMPs. It is worth noting that the authors of NDP report their performance in terms of the used samples rather than environment interactions (the original work only uses every fifth interaction). However, we believe that reporting the total number of environment interactions leads to a fairer comparison and also helps to explain the relatively poor performance of NDP in our experiments. For both MP3-BB and MP3-BB-PPO, we provide only the context information \mathbf{c} instead of leveraging the full state observation \mathbf{s} . The context information \mathbf{c} is a subset of the observation space that is randomly initialized after each reset and includes the stochastic elements, such as the goal or object positions. Unless otherwise specified, we measure the trajectory segment performance $R_{t:t+k}(\mathbf{w}, \mathbf{s})$ as the cumulative trajectory return. We evaluate our method on 20 different seeds and compute ten evaluation runs after each iteration. To report our results, we use the interquartile mean (IQM) with a 95% stratified bootstrap confidence interval and performance profiles where feasible Agar-

wal et al. (2021). For a detailed description of the hyperparameters used in the evaluation, please refer to Appendix E.

4.1 Black-Box Reinforcement Learning

Performance As an introductory task, we extend the reacher from OpenAI gym (Brockman et al., 2016) by using five actuated joints and limiting the context space, that is, the location of the goal, to $y \geq 0$. This results in an increased control complexity but slightly decreased task complexity. For a detailed environment description, please see Appendix C.1. We investigate two types of rewards: a dense reward equivalent to the original reacher, and a sparse reward that provides only the distance to the goal in the last episode time step. We study the sparse reward setting as it is better suited to generate energy-efficient motions. Yet, it is also more difficult to learn. While MP3-BB and MP3-BB-PPO can solve the task for both rewards, NDP and ES fail in both cases (Figures 3a and 3b). PPO and TRPL achieve a slightly better asymptotic performance than MP3-BB in the dense setting but are unable to consistently reach the goal for the sparse reward signal. Although SAC achieves a comparable performance to MP3-BB in the dense setting, it cannot leverage the sparse reward (see Appendix D). CMORE performs reasonably well, however, it is only able to cover part of context space due to its linear adaption strategy.

To demonstrate the learning capabilities of all algorithms in handling sparse rewards within a more complex scenario, we conduct evaluations on a box pushing task. The goal is to move a box to a given goal location and orientation using a simulated Franka Emika Panda. The goal location and orientation are randomized at the beginning of each episode. For a detailed environment description, please see Appendix C.2. Similar to the reacher task, we consider a dense reward signal and a temporal sparse reward signal. The dense reward is based on the position and orientation error for each time step, while the temporal sparse reward depends only on the distance errors at the last time step. We observed that the temporal sparse reward used in the original work leads to policies that pass through the target location at episode end. To address this issue, we increased the control cost penalty and introduced a joint velocity penalty at the episode end. We re-tuned baselines that exhibited competitive performance in the original setting to accommodate the new reward setup.

While MP3 and MP3-BB achieve the highest precision and sample efficiency in dense reward setting (Figure 4a), all SRL algorithms, excluding SAC, yielded acceptable performance at the end. The performance of SAC was adversely affected due to the penalties associated with constraint violation and control cost. In the sparse reward setting (Figure 4b), all the algorithms experience a certain degree of performance decline, while SRL algorithms encounter substantial performance degradation, the MP-based algorithms are capable of maintaining reasonable performance.

Although dense rewards may perform well in certain tasks (for instance, reacher and box-pushing), there are two main reasons to consider sparse rewards. Firstly, sparse rewards are usually easier to design, as we only need to consider the state at the last time step. Another reason is that dense rewards force the agent to reach the goal as fast as possible which typically yields energy inefficient motions. In contrast, sparse rewards only penalize the goal distance in the final time step, while accounting for energy costs in each time step.

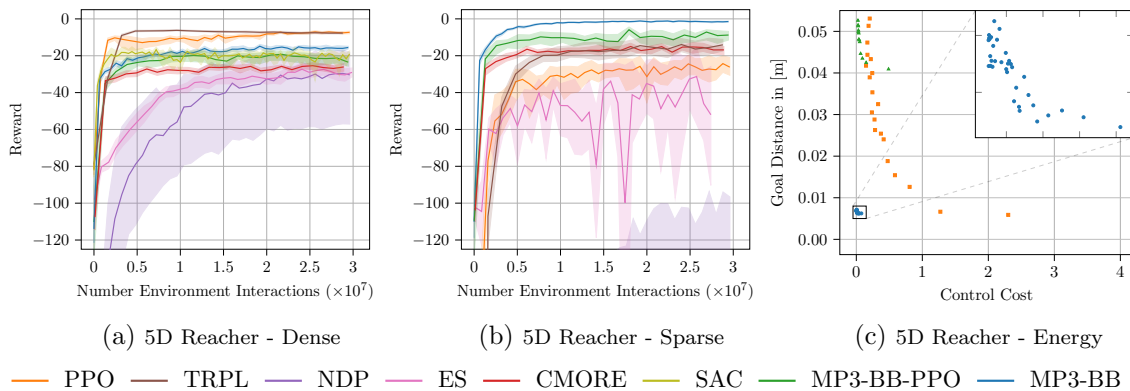


Figure 3: The figures (a) and (b) show the learning curve for the 5D reacher task with dense and sparse reward signals. Although TRPL and PPO achieve the best performance in the dense reward setting, both of them are struggling under the sparse reward setting. In contrast, MP3-BB achieves the best performance in the sparse reward setting. Figure (c) shows the tradeoff between the energy efficiency (sum of the squared control cost) and the task precision (distance to the goal at the last step). We average over 100 evaluation runs and all seeds and choose action penalty factors in the intervals $(0, 100]$. MP3-BB with sparse reward achieves the highest precision with much lower energy consumption compared to the PPO trained with the dense reward.

Energy Efficiency To illustrate the trade-off between precision and energy efficiency, we analyzed the final behaviors of both reward setups with different action penalty factors in the reward function. For each of these factors, we computed the average precision and energy consumption. Our results, shown in Figures 3c and 4c, demonstrate that decreasing the action penalty factor leads to higher task precision for all methods. However, for the dense reward, a high task precision comes with the cost of high energy penalties, whereas the sparse reward generates behavior of similar precision with one (box pushing) or even two (reacher) orders of magnitude less energy consumption. When analyzing the final behaviors, agents trained with the dense reward quickly move to the target and stay there, while the agents with the sparse reward reach the target only slightly before the specified end of the episode, resulting in a much slower, smoother, and more energy efficient motion.

Dealing with non-Markovian Rewards To assess the effectiveness of our method in complex reward settings, we test it with non-Markovian rewards, which are particularly useful for robot learning tasks that require the agent to use feedback from the full trajectory history. We first use a modified version of the OpenAI Gym hopper (Brockman et al., 2016), which aims to jump as high as possible and land at a target location (see Appendix C.3). The non-Markovian reward measures the highest point of the jump and the shortest distance to the target during the episode. We compare our approach with two other methods, CMORE and ES, which also use the non-Markovian reward. In addition, we train three different algorithms, PPO, SAC, and TRPL, using a Markovian version that provides height and target distance at each time step. For this setting, we performed extensive reward shaping to optimize for maximum height and minimum target distance. Overall, our results show

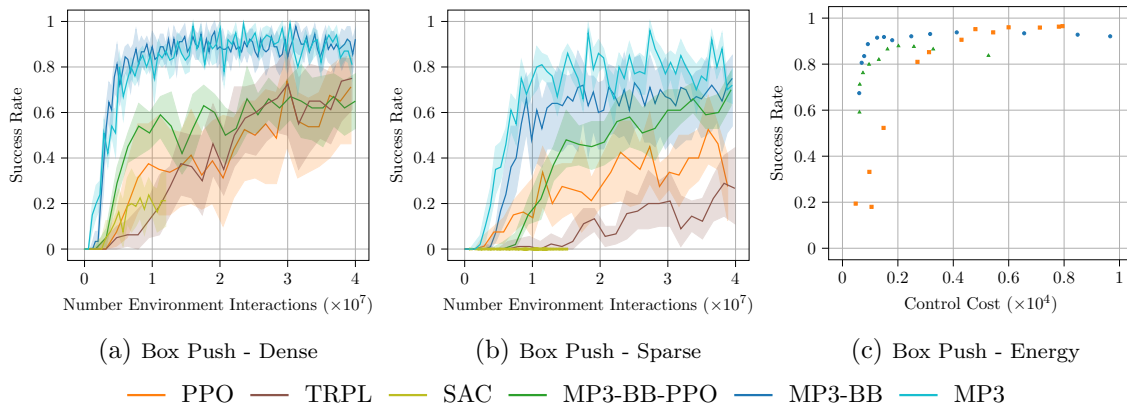


Figure 4: Figure (a) shows the learning curve for the box pushing task with a dense reward signal, while (b) with sparse reward signal. For the dense reward all the method except SAC achieve remarkable performance, while MP3 and MP3-BB achieve higher sample efficiency, this is due to the efficient exploration in parameters space. All methods suffer performance decrease with sparse reward signal (b), MP3 and MP3-BB are less influenced as they leverage highly temporal abstracted samples. MP3-BB achieve similar sample efficiency with MP3 because it can take advantage of more compact observations (context observation). Figure (c) shows the tradeoff between energy efficiency(sum of squared action) and task precision (success rate). Similar to the energy plot in 5D reacher task (Figure 3c), MP3-BB shows better energy-efficient behavior.

that MP3-BB achieves higher jump heights with smaller target distances compared to most other methods (Figures 5a and 5b). While MP3-BB-PPO and CMORE can match the target distance, SAC can even exceed it, none of them can reliably learn a good jump height. This can also be seen in the agent’s behavior. MP3-BB charges energy and then jumps only once, whereas the step-based methods try to maximize height in each time step, resulting in multiple jumps in one episode. This illustrates the need for non-Markovian rewards to describe certain behaviors.

To further strengthen the ability of MP3-BB in solving tasks with non-Markovian rewards, we conduct experiments in a Beer pong environment(Celik et al., 2022). In this task, the goal is to throw a ball into a cup at various locations on a table. The return depends on the entire trajectory of the ball, which can be calculated by using information such as table contacts or the minimum distance to the cup (a detailed description of the task can be found at Appendix C.4). However, directly training PPO on such a reward as well as designing a Markovian version of the reward is both challenging in this case. To address this issue and make PPO a stronger baseline, we simplified the task for PPO by fixing the ball release time and considering the time between the ball release and the end of the ball trajectory as the last time step, allowing PPO to compute the reward in a similar manner to the non-Markovian setting. This kind of simplification is unnecessary for ERL algorithms. We use MP3-BB and CMORE with the non-Markovian reward and learn the ball release time as an additional controller parameter. See results at Figure 5c. We see that both MP3-BB and MP3-BB-PPO are able to throw the ball into the cup, while PPO struggles. Even CMORE

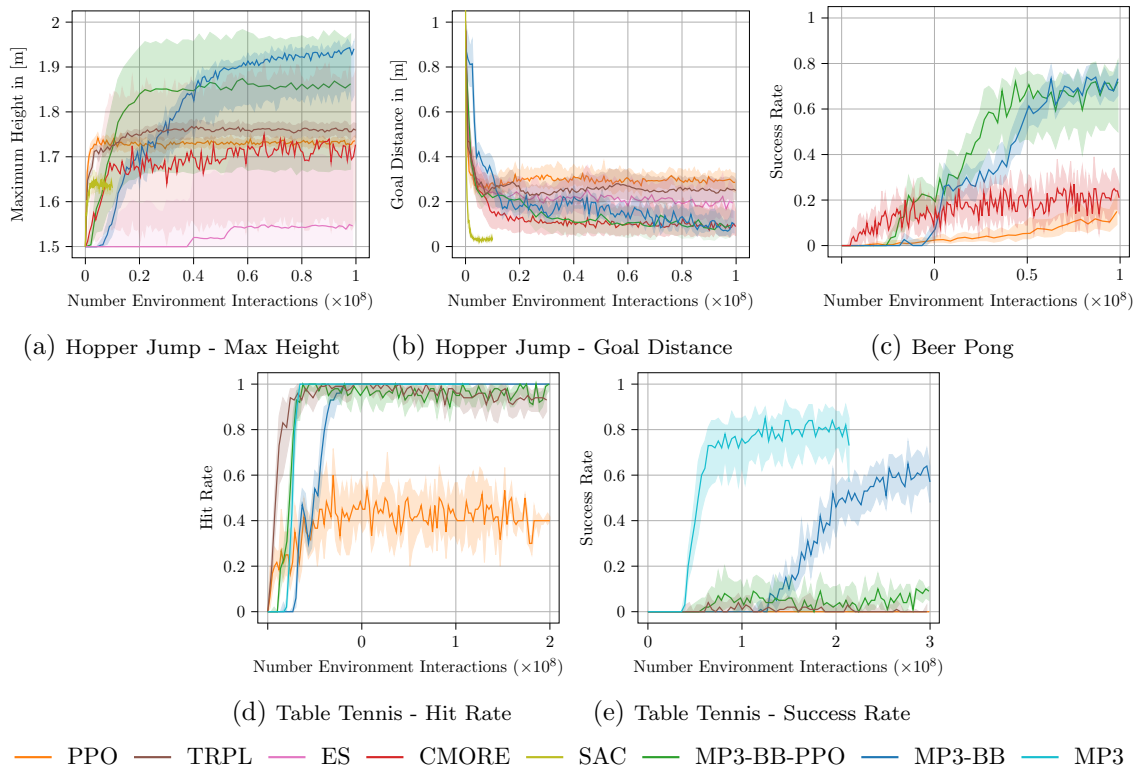


Figure 5: The figures (a) and (b) show the maximum jumping height of the hopper’s center of mass and the target distance, respectively. With the non-Markovian reward, the hopper can jump approximately 20cm higher with increased goal precision. Figure (c) shows the beer pong task, where PPO struggles to throw the ball into the cup, even with a fixed optimal release point, while MP3-BB can consistently succeed in the task with dynamic release points. The success and hit rate of the table tennis task are shown in (d) and (e), respectively. The episode is considered a success when the agent hits the ball and successfully returns the ball near the goal position. The results demonstrate that MP3-BB consistently hits the ball and returns it in most cases, and MP3 is even able to improve that performance further.

can throw the ball reliably, but only for a subset of the context space. Interestingly, we again observe that MP3-BB-PPO has a larger confidence interval compared to MP3-BB, indicating that it is not always able to solve the task consistently. This behavior is similar to the jumping task, where we also observed a larger confidence interval for MP3-BB-PPO.

Finally, we trained agents in a simulated table tennis environment (Celik et al., 2022). The context is four-dimensional, given by features of the incoming ball trajectory and the desired location for returning the ball (a detailed environment description is provided at Appendix C.5). The episode return depends on several factors, such as the minimum distance between the racket trajectory and ball trajectory, whether the racket hits the ball, and the distance error between the ball’s landing position and the target. It is worth noting that the agent’s action cannot influence the return after hitting the ball. Thus the return

after hitting is not conditioned on the action at the current step but on the previous actions, which poses a significant challenge for SRL algorithms. For step-based methods, we consider the time after hitting the ball as one time step, akin to the beer pong task. For the MP3 and MP3-BB approaches, we also learn the start time of the trajectory and the speed of the desired trajectory (which is a parameter of the MP). Both parameters help to learn the precise timing required to play table tennis. The results (Figures 5d and 5e) show that MP3-BB succeeds in hitting the ball and returning it within the vicinity of the goal in more than 60% of the cases. MP3-BB-PPO and TRPL can hit the ball but fail to return it accurately, PPO even fails to hit the ball consistently.

In summary, MP3-BB provides an effective solution for handling non-Markovian reward structures, which are often more natural and easier to define than engineered dense rewards. By leveraging these reward structures, the method can facilitate the learning of more sophisticated and efficient behaviors, leading to improved overall performance.

4.2 Large Scale Robot Manipulation

We also showcase our ability to learn high quality policies on the Meta-World benchmark suite (Yu et al., 2019). To verify our algorithms can adapt to task variations and solve tasks consistently, we use a more rigorous evaluation protocol compared to the one used by Yu et al. (2019). In contrast to using a fixed context for each episode, we randomly generate new contexts with each reset. Additionally, instead of considering any instance of success during the episode as a task solved, we consider a task successfully solved only if the last time step successfully solves the task. The last time step success metric rules out cases where the task is only momentarily solved but subsequently disrupted by random agent motion. We train individual policies for each environment but use the same hyperparameters. Our results (Figure 6a) show that PPO and TRPL achieve the best sample complexity, but MP3-BB performs competitively in terms of asymptotic performance and even outperforms PPO slightly in terms of asymptotic performance. Although the gap between PPO and MP3-BB in the aggregated view is relatively small, the corresponding performance profiles (Figure 6b) reveal that MP3-BB performs better above the 80% threshold. This means that MP3-BB finds more consistent solutions than PPO with higher precision and solves these tasks without failures. SAC performs similar to PPO, whereas NDP, ES, and MP3-BB-PPO are not achieving a competitive performance.

We conducted an additional ablation study in which we trained MP3-BB using sparse rewards, meaning only the final step reward of each episode was used. We denote this variant as MP3-BB sparse. While the interquartile mean (IQM) score is lower, it still able to complete 50% of the tasks with 100% success rate. This is a better performance than what we observed with PPO trained with dense rewards. Furthermore, the slope of the performance profile is quite small, indicating that nearly all the tasks that can be solved by the agent are solved with a high degree of accuracy.

4.3 Replanning with Movement Primitives

We evaluate our approach in the online replanning case by decreasing the planning horizon, such that $1 \leq k < T$, positioning it between SRL ($k = 1$) and ERL ($k = T$). This approach, which we refer to as MP3, offers two significant benefits. Firstly, it leads to

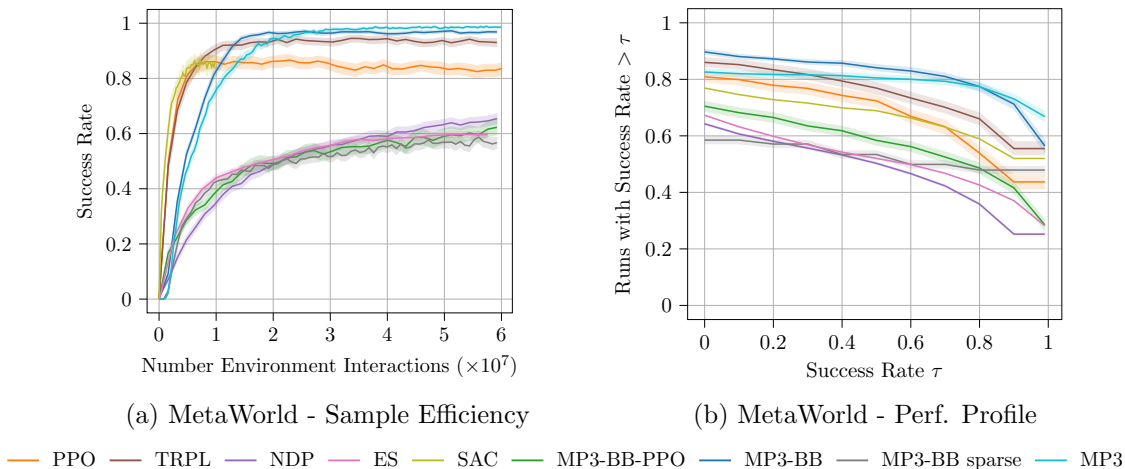


Figure 6: This Plot shows the success rate (a) for all 50 Meta-World tasks, and the corresponding performance profile (b), which is the fraction of runs that perform above the threshold given by the x-axis. Despite having lower sample efficiency, MP3-BB achieves a higher asymptotic policy quality than PPO. Finally, Movement Primitive-based Planning Policy (MP3) can further improve the asymptotic performance while being slightly less sample efficient. According to the performance profile (b), MP3-BB can solve more tasks (fewer runs with zero success rate) while MP3 can solve the tractable tasks more consistently (higher fraction of runs with $\geq 80\%$ success rate).

a more precise policy due to the closed-loop nature of the method. Secondly, it enables the handling of environmental dynamics through online replanning. However, there are two reasons why it is advantageous to consider it as a complementary approach rather than a complete replacement for MP3-BB. First, this design choice may limit the ability to address non-Markovian rewards, although we have also observed good results in this setting. Second, using replanning necessitates incorporating the internal proprioceptive state into the observation space, whereas the black-box setting can leverage a more concise observation space known as the context space.

Quality of the Learned Policy. We evaluated the performance of MP3 agents by conducting experiments in three challenging environments: the Meta-World benchmark suite (Yu et al., 2019) for large-scale robot manipulation, Box Pushing with dense and sparse rewards, and Table Tennis with non-Markovian reward.

We kept the same planning horizon (20% of the max episode length) in all 50 Meta-World environments. While the step-based methods achieved the best sample efficiency for Meta-World (Figure 7a), MP3 slightly outperforms the black-box approach and reaches the best asymptotic IQM score. The performance profile (Figure 6b) further indicates that although the number of unsolvable tasks remains constant, the quality of the solved tasks improves. In all the box-pushing experiments (Figure 7b), we kept the planning horizon to 25% of the max episode length. MP3 achieved the same performance with MP3-BB regarding success rate and sample efficiency in dense reward setting. In sparse reward setting, MP3 exhibited better precision and sample efficiency compared to MP3-BB. This is primarily due to the use

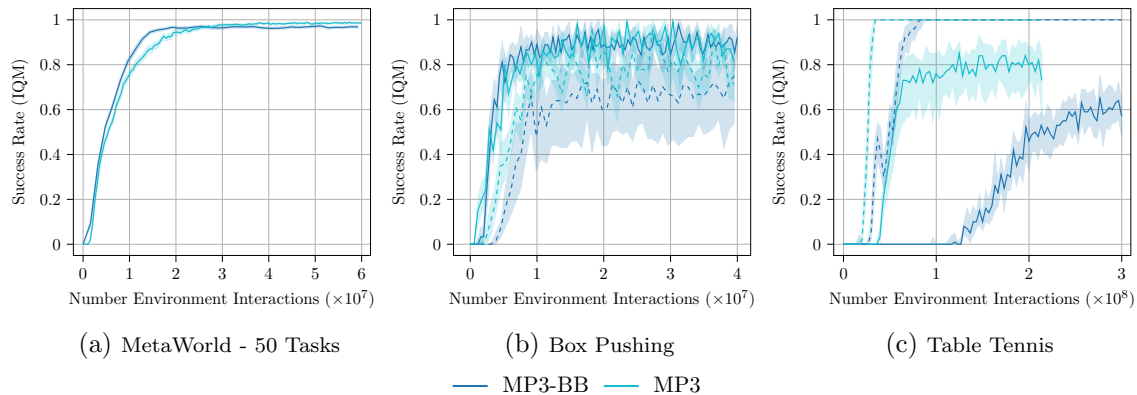


Figure 7: Figure (a) presents a comparison of the learning curves between MP3 and MP3-BB across Meta-World’s 50 tasks. Due to its closed-loop nature, MP3 achieves higher asymptotic performance with a marginal compromise in sample efficiency. This is attributed to the advantage of MP3-BB in utilizing a more compact observation space. Figure (b) shows the performance of both methods in the box pushing task, considering both dense (solid) and sparse (dashed) reward settings. While both methods achieve similar sample efficiency and asymptotic performance in dense reward settings, MP3 reaches a higher success rate in the sparse reward setting. Figure (c) demonstrates the hit rate (dashed) and success rate (solid) in the robot table tennis task. Both methods can consistently hit the ball, but MP3 outperforms MP3-BB by returning the ball with higher precision and requiring significantly fewer samples to converge.

of different MPs representations (ProDMPs for MP3 and ProMPs for MP3-BB). ProDMPs-based policies tend to generate trajectories with lower episode energy, which helps the agent to focus on the main target (move the box to the target) instead of regularized by the control penalty. We conducted an ablation in Figure 10d to verify this assumption.

While non-Markovian rewards cannot be used as freely as in the MP3-BB case, it is still possible to leverage them as long as the non-Markovian behavior is limited to one trajectory segment. For table tennis, we choose planning horizon k such that we ensure the last trajectory segment starts before the racket hits the ball. In this setting, MP3 learns table tennis skills with a better success rate and much fewer samples than MP3-BB (Figure 7c). In conclusion, we observed that the use of replanning yields better asymptotic performance in all cases while it can harm slightly the sample efficiency (observed in Meta-World experiments). We attribute this to the higher dimensional state space that must be considered in the replanning case compared to the black-box case.

Dealing with Uncertainties in the Environments. To demonstrate the robustness of MP3 in handling unforeseen events in the environment, we modified the box pushing and the table tennis tasks to include uncertainties that require incorporating feedback throughout the execution of the episode.

In the box-pushing experiments, we randomly switch to a new target position and orientation during execution after 20% of the max episode length. We compared the performance of our method against step-based PPO and TRPL in the dense reward setting. The re-

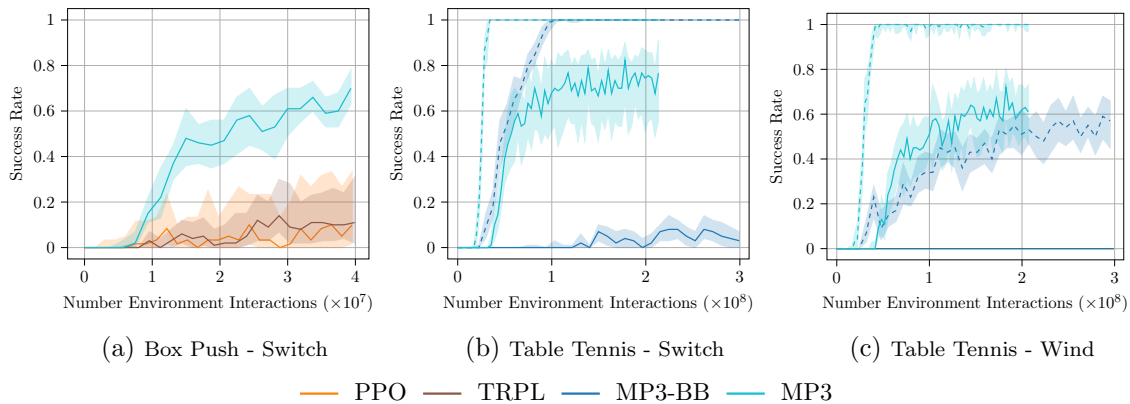


Figure 8: This figure displays the success rate of perturbed tasks with and without replanning. The success rate of box pushing with goal switching is shown at (a), as well as the success rate of table tennis with goal switching (b) and with wind (c). In the box pushing tasks (a), the solid lines represent learning curves of dense reward, while the dashed lines are learning curves from temporal-sparse reward. While step-based algorithms with dense reward already struggle in the easier 20% setting, MP3 trained with sparse reward can solve both settings with a remarkable success rate. In table tennis tasks (b) and (c), the solid lines represent the success rates, and the dashed lines are hit rate. MP3 can effectively handle changes in tasks and environmental perturbations. In contrast, the MP3-BB fails in these cases, as it only relies on a single observation at the beginning of the episode, which lacks critical information about the environment and task dynamics.

sults in Figure 8a show that MP3 achieved the best performance under this setting. To investigate the reasons behind this performance gap, we conducted a qualitative analysis of the trained policies with all three methods. We observed that the policies generated by PPO and TRPL accelerate much faster and keep a high velocity from the beginning of the episode, which makes adapting to the new targets more difficult with the presence of control cost penalty and limited episode length. On the other hand, the acceleration and velocity of MP3 agents are regularized by the ProDMP’s representation, leading to uniform motion, thus yielding an amenable success rate in this challenging goal-switching setting.

For the table tennis environment, we test two kinds of uncertainties. We compare MP3 only with the MP3-BB as the SRL algorithms have shown to be incapable of solving the table tennis task even in a static environment. Firstly, we modify the desired landing position of the ball, similar to the goal change for the box pushing task. Specifically, we initialize the desired landing position at a random location on the left side of the table. After half of the maximum episode steps, there is a 50% chance that the target landing position will change to a new random position on the right side of the table. Our results in Figure 8b suggest that the MP3 agent is able to adapt its behavior and return the ball to the new target point with high precision. In contrast, the MP3-BB agent, which only receives the initial observation containing the initial target position, can only hit the ball but cannot solve this task. While we would expect the MP3-BB agent to solve at least those cases where the goal is not altered, we found that the conflicting reward feedback hinders the

agent from learning high-quality policies. Secondly, we add wind to the environment by applying a random force to the ball, which is unknown to the agent and constant for an entire episode. However, the agent can still infer the underlying applied force according to the velocity of the ball, but only after observing the ball for a certain number of time steps. Due to the wind, the MP3-BB agent is not able to hit the ball consistently, while the MP3 agent slightly drops in performance but can still achieve reasonably good results (Figure 8c).

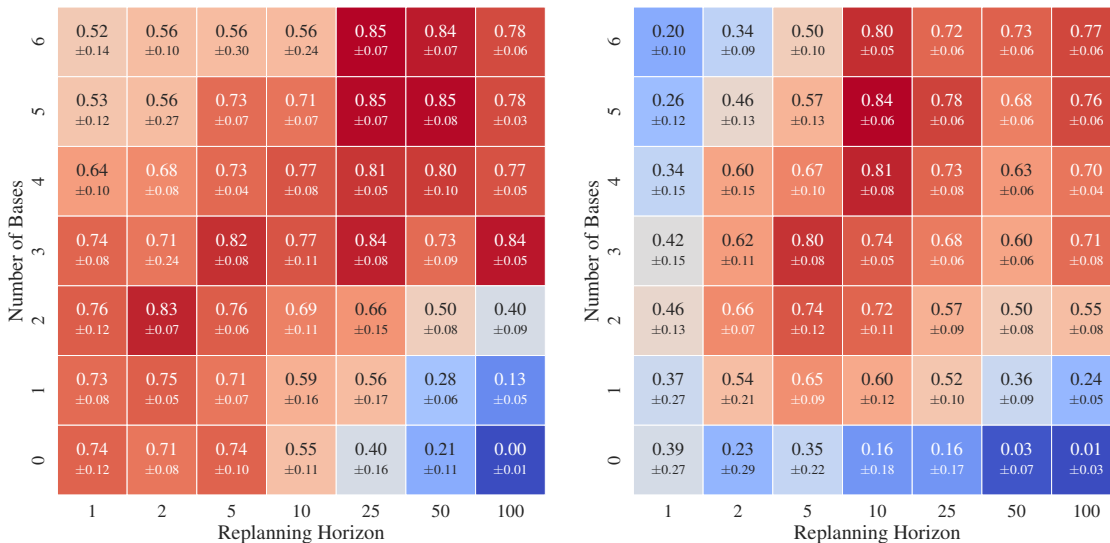
4.4 Ablation Studies

We conduct ablation studies to evaluate each component’s influence on the proposed method that aim to answer the following questions:

- Q1** What is the impact of varying the number of bases and the length of the replanning horizon on the performance of MP3?
- Q2** How does the performance of the non dynamic-based ProMP with replanning compare to MP3?
- Q3** Can the policy be effectively learned in the parameter space without incorporating proper trust regions?
- Q4** How does the performance of dynamic-based ProDMPs compare to non dynamic-based ProMPs in MP3-BB setting?

Firstly, we study the correlations between the number of bases of MPs and the length of the planning horizon (replanning steps) in Figure 9. We train agents in box pushing environments with both dense and sparse rewards, using different combinations of planning horizons $k \in \{1, 2, 5, 10, 25, 50, 100\}$ and the number of bases $N \in \{0, 1, 2, 3, 4, 5, 6\}$. A value of 0 for the number of bases indicates that the agent only uses the goal basis of the ProDMPs, leading to the same action space dimension as SRL algorithms. When the planning horizon is equal to 1, the learning objective of replanning reduces to a SRL objective. In this case, the only difference between replanning and SRL is that the agent explores the parameters space of the MP, which usually has a higher dimensionality $((N + 1) \times \text{DoF})$ compared to the action space that a step-based agent explores. Another special case is when the replanning horizon equals the episode length ($k = 100 = T$), which corresponds to the MP3-BB setting.

Q1 can be answered according to results in Figure 9. First, planning with a longer horizon requires a greater number of bases to achieve optimal performance. A longer planning horizon means less chance for the agent to adapt trajectories by adjusting the weights, limiting the ability to generate complex trajectories. This limitation, in turn, reduces performance in tasks that require fine manipulation, such as box pushing. Second, longer planning horizons contribute to improved performance in the (temporal) sparse reward setting. This is attributed to the usage of high temporal abstracted samples in the policy updates. However, it does not necessarily mean MP3-BB will always perform better in the sparse reward setting, as the black-box setting lacks the ability to correct its behavior due to the absence of the feedback signals from inter-execution observations.



(a) Median Success Rate for Dense Reward

(b) Median Success Rate for Sparse Reward

Figure 9: This figure shows the median success rate and standard deviation for different configurations of box pushing environments using dense (a) and sparse reward (b), with varying numbers of bases N and replanning horizons k . When $N = 0$, the weight bases are disabled, and only the goal basis of the ProDMP is used, with the action space dimension equal to that of SRL. $k = 1$ and $k = 100 = T$ correspond to SRL with MPs and MP3-BB, respectively. We evaluate each combination using ten random seeds and 20 contexts per seed. In general, the results suggest that: 1) longer planning horizons require more bases for optimal performance, 2) long planning horizons can help improve performance in sparse reward settings.

For **Q2**, we compare replanning with dynamic-based (ProDMPs) and non dynamic-based MPs (ProMPs) in Figures 10a and 10b. The results demonstrate that the policy with dynamic-based MPs yields a policy with a higher success rate and lower control cost. This is largely due to the fact that non-dynamic MPs can result in abrupt transitions between different planning segments, leading to discontinuities in the motion.

To address **Q3**, we evaluate policy search algorithms without trust regions in the replanning setting, and present the results in Figure 10c. In both dense and sparse reward settings of box pushing, MP3 outperforms MP3-PPO in terms of sample efficiency and success rate. The need for a more stable optimization and the higher dimensional nature of learning in parameter spaces could account for this observed improvement.

Finally, to answer **Q4**, we compare the performance between the black-box agent with ProDMPs and with ProMPs. The results in Figure 10d show that in dense and sparse reward settings, both algorithms' sample efficiency and success rate are similar. In the sparse reward setting, MP3-BB with ProMPs shows slightly higher asymptotic performance. This difference is due to the different shapes of bases, and we believe the minor performance gap can be mitigated by selecting MP's parameters that minimize the differences in bases. The

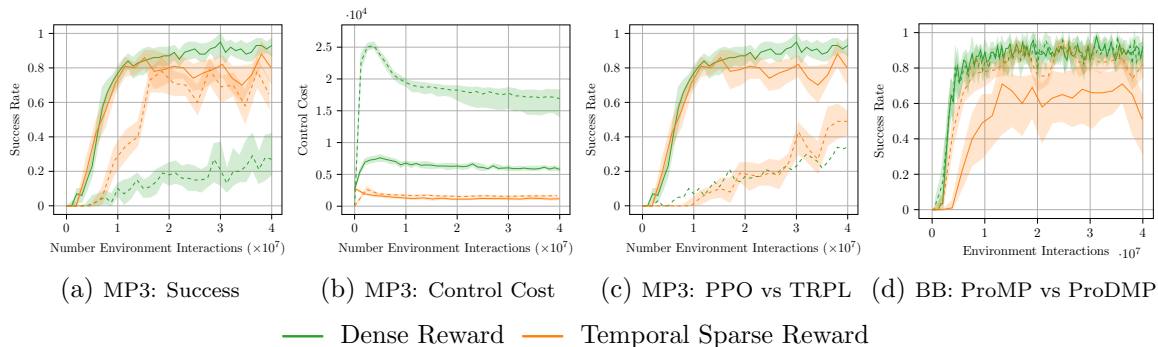


Figure 10: This figure presents an ablation study for MP3 and MP3-BB with different MPs and learning algorithms. The figures (a) and (b) show the success rate and episode control cost for the box-pushing task, respectively. Here, we compare MP3 with ProDMPs (solid) to MP3 with ProMPs (dashed) to show the need for ProDMPs when replanning. Figure (c) demonstrates the need for using TRPL in MP3 (solid). MP3-PPO with ProDMPs using replanning (dashed) on box pushing tasks is not able to achieve the same performance. Lastly, the figure (d) shows that MP3-BB with ProDMPs (dashed) is performing similarly to the MP3-BB with ProMPs (solid) in dense reward setting, and slightly better in the sparse reward setting.

overall results suggest that the types of MP make no significant difference in the black-box setting.

5 Conclusion and Limitations

Our work presents a new approach for combining SRL and ERL by integrating recent advancements in trust-region-based policy search (Otto et al., 2021) and MPs (Li et al., 2022). Unlike the commonly used step-based exploration in SRL, our method incorporates consistent and effective exploration at the trajectory level. This approach is a promising way to handle tasks with sparse and non-Markovian rewards, enabling a more intuitive reward design. Furthermore, our method showed competitive performance against state-of-the-art SRL algorithms in large-scale robot manipulation tasks, as confirmed by thorough empirical evaluations.

Although our proposed method shows promise, there remain some limitations that require addressing in future work. Firstly, our current approach only considers fixed-length planning horizons and relies solely on time-based replanning triggers. Yet, in real-world applications, it may be necessary to incorporate event-based replanning triggers, such as detecting unforeseen obstacles or changing targets. Therefore, we will investigate how to integrate event-based triggers into our method in the future. Secondly, our method, and ERL approaches in general, typically require more interaction time than SRL in dense reward settings. This is mainly due to the encapsulation of temporal-correlated information in highly abstracted samples. To address this issue, we will leverage the information within each planning segment to improve efficiency. Lastly, our evaluation of the Meta-World benchmark suite identified that most failure cases occur in tasks requiring sub-goal achievement

and skill sequencing. Therefore, we will investigate how to achieve long-horizon planning by incorporating sub-goals into our framework in future work.

Acknowledgments and Disclosure of Funding

The presented work was funded by the Carl Zeiss Foundation through the Project JuBot (Jung Bleiben mit Robotern), the Helmholtz Association of German Research Centers and by the Deutsche Forschungsgemeinschaft (DFG), German Research Foundation under Grant 448648559 (Intuitive Robot Intelligence). This work was supported by the state of Baden-Württemberg through bwHPC. This work was performed on the HoreKa supercomputer funded by the Ministry of Science, Research and the Arts Baden-Württemberg and by the Federal Ministry of Education and Research.

References

- Abbas Abdolmaleki, Rudolf Lioutikov, Jan R Peters, Nuno Lau, Luis Pualo Reis, and Gerhard Neumann. Model-based relative entropy stochastic search. *Advances in Neural Information Processing Systems*, 28, 2015.
- Abbas Abdolmaleki, David Simões, Nuno Lau, Luís Paulo Reis, and Gerhard Neumann. Contextual direct policy search. *Journal of Intelligent & Robotic Systems*, 96(2):141–157, 2019.
- Rishabh Agarwal, Max Schwarzer, Pablo Samuel Castro, Aaron Courville, and Marc G Bellemare. Deep reinforcement learning at the edge of the statistical precipice. *Advances in Neural Information Processing Systems*, 2021.
- Akshay Agrawal, Brandon Amos, Shane Barratt, Stephen Boyd, Steven Diamond, and J Zico Kolter. Differentiable convex optimization layers. *Advances in neural information processing systems*, 32, 2019.
- Riad Akrou, Joni Pajarinen, Jan Peters, and Gerhard Neumann. Projections for approximate policy iteration algorithms. In *Proceedings of Machine Learning Research*, pages 181–190, 2019.
- Shikhar Bahl, Mustafa Mukadam, Abhinav Gupta, and Deepak Pathak. Neural dynamic policies for end-to-end sensorimotor learning. *Advances in Neural Information Processing Systems*, 12 2020. URL <https://arxiv.org/abs/2012.02788v1>.
- Christopher Berner, Greg Brockman, Brooke Chan, Vicki Cheung, Przemyslaw Debiak, Christy Dennison, David Farhi, Quirin Fischer, Shariq Hashme, Chris Hesse, et al. Dota 2 with large scale deep reinforcement learning. *arXiv preprint arXiv:1912.06680*, 2019.
- Florian Brandherm, Jan Peters, Gerhard Neumann, and Riad Akrou. Learning replanning policies with direct policy search. *IEEE Robotics and Automation Letters*, 4(2):2196–2203, 2019.

- Alex Braylan, Mark Hollenbeck, Elliot Meyerson, and Risto Miikkulainen. Frame skip is a powerful parameter for learning to play atari. In *Workshops at the Twenty-Ninth AAAI Conference on Artificial Intelligence*, 2015.
- Greg Brockman, Vicki Cheung, Ludwig Pettersson, Jonas Schneider, John Schulman, Jie Tang, and Wojciech Zaremba. Openai gym, 2016.
- Onur Celik, Dongzhuoran Zhou, Ge Li, Philipp Becker, and Gerhard Neumann. Specializing versatile skill libraries using local mixture of experts. In *Conference on Robot Learning*, pages 1423–1433. PMLR, 2022.
- Patryk Chrabaszcz, Ilya Loshchilov, and Frank Hutter. Back to basics: Benchmarking canonical evolution strategies for playing atari. In *IJCAI*, 2018.
- Murtaza Dalal, Deepak Pathak, and Russ R Salakhutdinov. Accelerating robotic reinforcement learning via parameterized action primitives. *Advances in Neural Information Processing Systems*, 34:21847–21859, 2021.
- Christian Daniel, Gerhard Neumann, and Jan Peters. Hierarchical relative entropy policy search. In *Artificial Intelligence and Statistics*, pages 273–281. PMLR, 2012.
- Marc Peter Deisenroth, Gerhard Neumann, Jan Peters, et al. A survey on policy search for robotics. *Foundations and trends in Robotics*, 2(1-2):388–403, 2013.
- Logan Engstrom, Andrew Ilyas, Shibani Santurkar, Dimitris Tsipras, Firdaus Janoos, Larry Rudolph, and Aleksander Madry. Implementation Matters in Deep Policy Gradients: A Case Study on PPO and TRPO. In *International Conference on Learning Representations*, 2020. URL <http://arxiv.org/abs/2005.12729>.
- Michele Ginesi, Daniele Meli, Hirenkumar Nakawala, Andrea Roberti, and Paolo Fiorini. A knowledge-based framework for task automation in surgery. In *2019 19th International Conference on Advanced Robotics (ICAR)*, pages 37–42. IEEE, 2019.
- Sebastian Gomez-Gonzalez, Gerhard Neumann, Bernhard Schölkopf, and Jan Peters. Using probabilistic movement primitives for striking movements. In *2016 IEEE-RAS 16th International Conference on Humanoid Robots (Humanoids)*, pages 502–508. IEEE, 2016.
- Tuomas Haarnoja, Aurick Zhou, Pieter Abbeel, and Sergey Levine. Soft actor-critic: Off-policy maximum entropy deep reinforcement learning with a stochastic actor. In *International conference on machine learning*, pages 1861–1870. PMLR, 2018.
- N. Hansen and A. Ostermeier. Completely derandomized self-adaptation in evolution strategies. *Evolutionary computation*, 9(2):159–195, 2001.
- Auke Jan Ijspeert, Jun Nakanishi, Heiko Hoffmann, Peter Pastor, and Stefan Schaal. Dynamical Movement Primitives: Learning Attractor Models for Motor Behaviors. *Neural Computation*, 25(2), 2013.

- Jens Kober and Jan Peters. Policy search for motor primitives in robotics. In D. Koller, D. Schuurmans, Y. Bengio, and L. Bottou, editors, *Advances in Neural Information Processing Systems*, volume 21. Curran Associates, Inc., 2008. URL <https://proceedings.neurips.cc/paper/2008/file/7647966b7343c29048673252e490f736-Paper.pdf>.
- Petar Kormushev, Sylvain Calinon, and Darwin G Caldwell. Robot motor skill coordination with em-based reinforcement learning. In *2010 IEEE/RSJ international conference on intelligent robots and systems*, pages 3232–3237. IEEE, 2010.
- Petar Kormushev, Sylvain Calinon, and Darwin G Caldwell. Reinforcement learning in robotics: Applications and real-world challenges. *Robotics*, 2(3):122–148, 2013.
- Andras Kupcsik, Marc P. Deisenroth, Jan Peters, Loh Ai Poha, Prahlad Vadakkepata, and Gerhard Neumann. Model-based contextual policy search for data-efficient generalization of robot skills. *Artificial Intelligence*, 247:415–439, 2017. doi: 10.1016/j.artint.2014.11.005. URL http://eprints.lincoln.ac.uk/25774/1/Kupcsik_AIJ_2015.pdf. Impact Factor: 3.333.
- Hyeonbeom Lee, Hoseong Seo, and Hyeong-Geun Kim. Trajectory optimization and re-planning framework for a micro air vehicle in cluttered environments. *Ieee Access*, 8: 135406–135415, 2020.
- Ge Li, Zeqi Jin, Michael Volpp, Fabian Otto, Rudolf Lioutikov, and Gerhard Neumann. Prodmps: A unified perspective on dynamic and probabilistic movement primitives. *arXiv preprint arXiv:2210.01531*, 2022.
- Zhijun Li, Ting Zhao, Fei Chen, Yingbai Hu, Chun-Yi Su, and Toshio Fukuda. Reinforcement learning of manipulation and grasping using dynamical movement primitives for a humanoidlike mobile manipulator. *IEEE/ASME Transactions on Mechatronics*, 23(1): 121–131, 2017.
- Guilherme Maeda, Marco Ewerton, Rudolf Lioutikov, Heni Ben Amor, Jan Peters, and Gerhard Neumann. Learning interaction for collaborative tasks with probabilistic movement primitives. In *2014 IEEE-RAS International Conference on Humanoid Robots*, pages 527–534. IEEE, 2014.
- Horia Mania, Aurelia Guy, and Benjamin Recht. Simple random search of static linear policies is competitive for reinforcement learning. In S. Bengio, H. Wallach, H. Larochelle, K. Grauman, N. Cesa-Bianchi, and R. Garnett, editors, *Advances in Neural Information Processing Systems*, volume 31. Curran Associates, Inc., 2018. URL <https://proceedings.neurips.cc/paper/2018/file/7634ea65a4e6d9041cfd3f7de18e334a-Paper.pdf>.
- Shie Mannor, Reuven Y Rubinstein, and Yoichi Gat. The cross entropy method for fast policy search. In *Proceedings of the 20th International Conference on Machine Learning (ICML-03)*, pages 512–519, 2003.
- Katharina Mülling, Jens Kober, Oliver Kroemer, and Jan Peters. Learning to select and generalize striking movements in robot table tennis. *The International Journal of Robotics Research*, 32(3):263–279, 2013.

- R OpenAI. Gpt-4 technical report. *arXiv*, 2023.
- Fabian Otto, Philipp Becker, Ngo Anh Vien, Hanna Carolin Ziesche, and Gerhard Neumann. Differentiable trust region layers for deep reinforcement learning. In *International Conference on Learning Representations*, 2021.
- Fabian Otto, Onur Celik, Hongyi Zhou, Hanna Ziesche, Ngo Anh Vien, and Gerhard Neumann. Deep black-box reinforcement learning with movement primitives. *arXiv preprint arXiv:2210.09622*, 2022.
- Rok Pahič, Andrej Gams, Aleš Ude, and Jun Morimoto. Deep encoder-decoder networks for mapping raw images to dynamic movement primitives. In *2018 IEEE International Conference on Robotics and Automation*, 2018.
- Rok Pahič, Barry Ridge, Andrej Gams, Jun Morimoto, and Aleš Ude. Training of deep neural networks for the generation of dynamic movement primitives. *Neural Networks*, 2020.
- Alexandros Paraschos, Christian Daniel, Jan R Peters, and Gerhard Neumann. Probabilistic movement primitives. In C. J. C. Burges, L. Bottou, M. Welling, Z. Ghahramani, and K. Q. Weinberger, editors, *Advances in Neural Information Processing Systems*, volume 26. Curran Associates, Inc., 2013. URL <https://proceedings.neurips.cc/paper/2013/file/e53a0a2978c28872a4505bdb51db06dc-Paper.pdf>.
- Leonel Rozo and Vedant Dave. Orientation probabilistic movement primitives on riemannian manifolds. In *Conference on Robot Learning*, pages 373–383. PMLR, 2022.
- Tim Salimans, Jonathan Ho, Xi Chen, Szymon Sidor, and Ilya Sutskever. Evolution strategies as a scalable alternative to reinforcement learning. *arXiv preprint arXiv:1703.03864*, 2017.
- Stefan Schaal. *Dynamic Movement Primitives -A Framework for Motor Control in Humans and Humanoid Robotics*, pages 261–280. Springer Tokyo, Tokyo, 2006. ISBN 978-4-431-31381-6. doi: 10.1007/4-431-31381-8_23. URL https://doi.org/10.1007/4-431-31381-8_23.
- Stefan Schaal, Jan Peters, Jun Nakanishi, and Auke Ijspeert. Learning movement primitives. In *Robotics research. the eleventh international symposium*, pages 561–572. Springer, 2005.
- John Schulman, Sergey Levine, Pieter Abbeel, Michael Jordan, and Philipp Moritz. Trust Region Policy Optimization. In *Proceedings of Machine Learning Research*, pages 1889–1897, 2015. URL <http://proceedings.mlr.press/v37/schulman15.html>.
- John Schulman, Philipp Moritz, Sergey Levine, Michael Jordan, and Pieter Abbeel. High-dimensional continuous control using generalized advantage estimation. In *Proceedings of the International Conference on Learning Representations (ICLR)*, 2016.

- John Schulman, Filip Wolski, Prafulla Dhariwal, Alec Radford, and Oleg Klimov. Proximal Policy Optimization Algorithms. In *arXiv preprint*, 2017. URL <http://arxiv.org/abs/1707.06347>.
- F. Sehnke, C. Osendorfer, T. Rückstieß, A. Graves, J. Peters, and J. Schmidhuber. Parameter-exploring policy gradients. *Neural Networks*, 21(4):551–559, May 2010. doi: 10.1016/j.neunet.2009.12.004.
- Freek Stulp and Olivier Sigaud. Path integral policy improvement with covariance matrix adaptation. In *Proceedings of the 29th International Conference on International Conference on Machine Learning, ICML’12*, page 1547–1554, Madison, WI, USA, 2012a. Omnipress. ISBN 9781450312851.
- Freek Stulp and Olivier Sigaud. Policy improvement methods: Between black-box optimization and episodic reinforcement learning. 2012b.
- Richard S Sutton, David McAllester, Satinder Singh, and Yishay Mansour. Policy gradient methods for reinforcement learning with function approximation. In S. Solla, T. Leen, and K. Müller, editors, *Advances in Neural Information Processing Systems*, volume 12. MIT Press, 1999. URL <https://proceedings.neurips.cc/paper/1999/file/464d828b85b0bed98e80ade0a5c43b0f-Paper.pdf>.
- Voot Tangkaratt, Herke van Hoof, Simone Parisi, Gerhard Neumann, Jan Peters, and Masashi Sugiyama. Policy search with high-dimensional context variables. In *Proceedings of the AAAI Conference on Artificial Intelligence*, volume 31, 2017.
- Daan Wierstra, Tom Schaul, Tobias Glasmachers, Yi Sun, Jan Peters, and Jürgen Schmidhuber. Natural evolution strategies. *The Journal of Machine Learning Research*, 15(1): 949–980, 2014.
- Ronald J Williams. Simple statistical gradient-following algorithms for connectionist reinforcement learning. *Machine learning*, 8(3):229–256, 1992.
- Tianhe Yu, Deirdre Quillen, Zhanpeng He, Ryan Julian, Karol Hausman, Chelsea Finn, and Sergey Levine. Meta-world: A benchmark and evaluation for multi-task and meta reinforcement learning. In *Conference on Robot Learning (CoRL)*, 2019. URL <https://arxiv.org/abs/1910.10897>.
- Oussama Zenkri, Ngo Anh Vien, and Gerhard Neumann. Hierarchical policy learning for mechanical search. In *2022 International Conference on Robotics and Automation (ICRA)*, pages 1954–1960. IEEE, 2022.

Appendix A. Derivations of probabilistic dynamic movement primitive.

In this section, we will briefly present the main derivations of ProDMPs. We start with the fundamental aspects of DMPs and then derive ProDMPs from the analytical solution of the DMPs' ODE. Finally, we present the solution to a initial value problem of the ODE, which allows us to perform smooth replanning during trajectory execution in a computationally efficient manner. For the sake of simplicity, we introduce the approach by means of a 1-DoF dynamical system. For higher DoF systems, we refer to the original paper by Li et al. (2022).

dynamic movement primitive Schaal (2006); Ijspeert et al. (2013) model a single movement execution as a trajectory $\lambda = [y_t]_{t=0:T}$ using a second-order linear dynamical system with a non-linear forcing function f ,

$$\tau^2 \ddot{y} = \alpha(\beta(g - y) - \tau \dot{y}) + f(x), \quad f(x) = x \frac{\sum \varphi_i(x) w_i}{\sum \varphi_i(x)} = x \boldsymbol{\varphi}_x^T \mathbf{w}, \quad (8)$$

where $y = y(t)$, $\dot{y} = dy/dt$, $\ddot{y} = d^2y/dt^2$ represent the position, velocity, and acceleration of the system at time step t , respectively. α and β are spring-damper constants, g is a goal attractor, and τ is a time constant that can be used to adjust the execution speed of the resulting trajectory. To achieve goal convergence, DMPs define the forcing function based on an exponentially decaying phase variable $x(t) = \exp(-\alpha_x/\tau t)$, where $\varphi_i(x)$ represents the (unnormalized) basis functions. The shape of the trajectory as it converges to the goal is controlled by the weights $w_i \in \mathbf{w}$, $i = 1 \dots N$. The trajectory of the motion λ is obtained by integrating the system numerically from the starting time to the target time point. However, this process is often computationally expensive.

Solving the dynamic movement primitives' underlying ODE. Li et al. recognize that the governing equation of DMPs, given in Eq.(8), has an analytical solution, as it is a second-order linear non-homogeneous ODE with constant coefficients. To better convey this method, the ODE and its homogeneous counterpart can be rewritten in a standard form as:

$$\text{Non-homo. ODE: } \ddot{y} + \frac{\alpha}{\tau} \dot{y} + \frac{\alpha\beta}{\tau^2} y = \frac{f(x)}{\tau^2} + \frac{\alpha\beta}{\tau^2} g \equiv F(x, g), \quad (9)$$

$$\text{Homo. ODE: } \ddot{y} + \frac{\alpha}{\tau} \dot{y} + \frac{\alpha\beta}{\tau^2} y = 0. \quad (10)$$

With appropriate configuration of the spring-damper coefficients, i.e., $\beta = \alpha/4$ (Schaal (2006); Ijspeert et al. (2013)), the system is critically damped and the motion generated by the DMPs will settle to the target position smoothly and efficiently. The analytical solution of Eq. (9) in this case takes the form

$$y = c_1 y_1 + c_2 y_2 - y_1 \int \frac{y_2 F}{Y} dt + y_2 \int \frac{y_1 F}{Y} dt, \quad Y = y_1 \dot{y}_2 - \dot{y}_1 y_2, \quad (11)$$

$$y_1 = y_1(t) = \exp\left(-\frac{\alpha}{2\tau} t\right), \quad y_2 = y_2(t) = t \exp\left(-\frac{\alpha}{2\tau} t\right), \quad (12)$$

where y_1 and y_2 are the complementary functions of the homogeneous function in Eq. (10) and \dot{y}_1 , \dot{y}_2 their corresponding derivatives w.r.t. time. By utilizing the fundamental of

calculus, which states that $\int h(t)dt = \int_0^t h(t')dt' + c$, where $c \in \mathbb{R}$ is a constant, the two indefinite integrals in Eq. (11) can be transformed into two definite integrals. During this transformation, the learnable parameters \mathbf{w} and g which control the shape of the trajectory, can be extracted from the resulting definite integrals. Finally, the trajectory position and velocity can be expressed in a compact matrix form as

$$y = c_1 y_1 + c_2 y_2 + \begin{bmatrix} y_2 \mathbf{p}_2 - y_1 \mathbf{p}_1 & y_2 q_2 - y_1 q_1 \end{bmatrix} \begin{bmatrix} \mathbf{w} \\ g \end{bmatrix} \quad (13)$$

$$\dot{y} = c_1 \dot{y}_1 + c_2 \dot{y}_2 + \begin{bmatrix} \dot{y}_2 \mathbf{p}_2 - \dot{y}_1 \mathbf{p}_1 & \dot{y}_2 q_2 - \dot{y}_1 q_1 \end{bmatrix} \begin{bmatrix} \mathbf{w} \\ g \end{bmatrix}, \quad (14)$$

where $\mathbf{p}_1, \mathbf{p}_2, q_1, q_2$ represent the elements used to formulate the definite integrals in the matrix form, as

$$\mathbf{p}_1(t) = \frac{1}{\tau^2} \int_0^t t' \exp\left(\frac{\alpha}{2\tau} t'\right) x(t') \boldsymbol{\varphi}_x^\top dt', \quad \mathbf{p}_2(t) = \frac{1}{\tau^2} \int_0^t \exp\left(\frac{\alpha}{2\tau} t'\right) x(t') \boldsymbol{\varphi}_x^\top dt', \quad (15)$$

$$q_1(t) = \left(\frac{\alpha}{2\tau} t - 1\right) \exp\left(\frac{\alpha}{2\tau} t\right) + 1, \quad q_2(t) = \frac{\alpha}{2\tau} \left[\exp\left(\frac{\alpha}{2\tau} t\right) - 1\right]. \quad (16)$$

It is worth noting that, despite the closed form solution for q_1 and q_2 , \mathbf{p}_1 and \mathbf{p}_2 cannot be obtained analytically because of the complex nature of the $\boldsymbol{\varphi}_x$. As a result, they must be computed numerically. However, the extraction of the learnable parameters \mathbf{w} and g from the integrals in Eq. (13) and (14) enables the sharing of the remaining integrals among all trajectories to be generated. In other words, these integrals can be pre-computed offline and used as constant functions during online trajectory computation, which significantly simplifies the trajectory generation procedure and speeds it up. These remaining integrals are referred to as the position basis $\Phi(t)$ and velocity basis $\dot{\Phi}(t)$, and the ProDMPs represent the position and velocity in a similar manner of ProMPs as:

$$y(t) = c_1 y_1(t) + c_2 y_2(t) + \Phi(t)^\top \mathbf{w}_g, \quad \dot{y}(t) = c_1 \dot{y}_1(t) + c_2 \dot{y}_2(t) + \dot{\Phi}(t)^\top \mathbf{w}_g, \quad (3.1)$$

where \mathbf{w}_g is a concatenation vector containing \mathbf{w} and g .

Solve the initial value problem. To compute the coefficients c_1 and c_2 , a solution to the initial value problem represented by the Eq.(3.1) must be found. Li et al. suggest using the current robot state, which consists of the robot's position and velocity (y_b, \dot{y}_b) at the replanning time step t_b , as the natural condition for ensuring a smooth transition between the previous and newly generated trajectory. We denote the values of the complementary functions and their derivatives at time t_b as $y_{1_b}, y_{2_b}, \dot{y}_{1_b}, \dot{y}_{2_b}$, and the values of the position and velocity basis functions as $\Phi_b, \dot{\Phi}_b$. By substituting these values into Eq.(3.1), c_1 and c_2 can be calculated as:

$$\begin{bmatrix} c_1 \\ c_2 \end{bmatrix} = \begin{bmatrix} \frac{\dot{y}_{2_b} y_b - y_{2_b} \dot{y}_b}{y_{1_b} \dot{y}_{2_b} - y_{2_b} \dot{y}_{1_b}} + \frac{y_{2_b} \dot{\Phi}_b^\top - \dot{y}_{2_b} \Phi_b^\top}{y_{1_b} \dot{y}_{2_b} - y_{2_b} \dot{y}_{1_b}} \mathbf{w}_g \\ \frac{y_{1_b} \dot{y}_b - \dot{y}_{1_b} y_b}{y_{1_b} \dot{y}_{2_b} - y_{2_b} \dot{y}_{1_b}} + \frac{\dot{y}_{1_b} \Phi_b^\top - y_{1_b} \dot{\Phi}_b^\top}{y_{1_b} \dot{y}_{2_b} - y_{2_b} \dot{y}_{1_b}} \mathbf{w}_g \end{bmatrix}. \quad (17)$$

Appendix B. Trust Region Projection Layers with KL-Divergence

As already mentioned in the main text, TRPLs Otto et al. (2021) present a scalable and mathematically sound approach for enforcing trust regions in step-based deep RL. The layer takes the output of a standard Gaussian policy as input in terms of mean $\boldsymbol{\mu}$ and variance $\boldsymbol{\Sigma}$ and projects it into the trust region if the given mean and variance violate their respective bounds. This projection is done for each input state individually. Subsequently, the projected Gaussian policy distribution with parameters $\tilde{\boldsymbol{\mu}}, \tilde{\boldsymbol{\Sigma}}$ is used for any further steps, e.g. for sampling and/or loss computation. Formally, the layer solves the following two optimization problems for each state \mathbf{s}

$$\arg \min_{\tilde{\boldsymbol{\mu}}_s} d_{\text{mean}}(\tilde{\boldsymbol{\mu}}_s, \boldsymbol{\mu}(\mathbf{s})), \quad \text{s.t.} \quad d_{\text{mean}}(\tilde{\boldsymbol{\mu}}_s, \boldsymbol{\mu}_{\text{old}}(\mathbf{s})) \leq \epsilon_{\boldsymbol{\mu}}, \quad \text{and} \quad (18)$$

$$\arg \min_{\tilde{\boldsymbol{\Sigma}}_s} d_{\text{cov}}(\tilde{\boldsymbol{\Sigma}}_s, \boldsymbol{\Sigma}(\mathbf{s})), \quad \text{s.t.} \quad d_{\text{cov}}(\tilde{\boldsymbol{\Sigma}}_s, \boldsymbol{\Sigma}_{\text{old}}(\mathbf{s})) \leq \epsilon_{\boldsymbol{\Sigma}}, \quad (19)$$

where $\tilde{\boldsymbol{\mu}}_s$ and $\tilde{\boldsymbol{\Sigma}}_s$ are the optimization variables for input state \mathbf{s} and $\epsilon_{\boldsymbol{\mu}}$ and $\epsilon_{\boldsymbol{\Sigma}}$ are the trust region bounds for mean and covariance, respectively. Finally, $\boldsymbol{\mu}_{\text{old}}$ and $\boldsymbol{\Sigma}_{\text{old}}$ are the reference mean and covariance for the trust region and d_{mean} as well as d_{cov} are the similarity metrics for the mean and covariance of a decomposable distance or divergence measure. As we only leverage the KL-divergence projection, we will provide only details for this particular projection below. For the other two projections we refer the reader to Otto et al. (2021). Inserting the mean part of the Gaussian KL divergence into Equation 18 yields

$$\arg \min_{\tilde{\boldsymbol{\mu}}} (\boldsymbol{\mu} - \tilde{\boldsymbol{\mu}})^{\text{T}} \boldsymbol{\Sigma}_{\text{old}}^{-1} (\boldsymbol{\mu} - \tilde{\boldsymbol{\mu}}) \quad \text{s.t.} \quad (\boldsymbol{\mu}_{\text{old}} - \tilde{\boldsymbol{\mu}})^{\text{T}} \boldsymbol{\Sigma}_{\text{old}}^{-1} (\boldsymbol{\mu}_{\text{old}} - \tilde{\boldsymbol{\mu}}) \leq \epsilon_{\boldsymbol{\mu}}.$$

After differentiating the dual w.r.t. $\tilde{\boldsymbol{\mu}}$, we can solve for the projected mean

$$\tilde{\boldsymbol{\mu}} = \frac{\boldsymbol{\mu} + \omega \boldsymbol{\mu}_{\text{old}}}{1 + \omega} \quad \text{with} \quad \omega = \sqrt{\frac{(\boldsymbol{\mu}_{\text{old}} - \boldsymbol{\mu})^{\text{T}} \boldsymbol{\Sigma}_{\text{old}}^{-1} (\boldsymbol{\mu}_{\text{old}} - \boldsymbol{\mu})}{\epsilon_{\boldsymbol{\mu}}}} - 1,$$

leveraging the optimal Lagrange multiplier ω . Similarly, we can insert the covariance part of the Gaussian KL divergence into Equation 19, which results in

$$\arg \min_{\tilde{\boldsymbol{\Sigma}}} \text{tr}(\boldsymbol{\Sigma}^{-1} \tilde{\boldsymbol{\Sigma}}) + \log \frac{|\boldsymbol{\Sigma}|}{|\tilde{\boldsymbol{\Sigma}}|}, \quad \text{s.t.} \quad \text{tr}(\boldsymbol{\Sigma}_{\text{old}}^{-1} \tilde{\boldsymbol{\Sigma}}) - d + \log \frac{|\boldsymbol{\Sigma}_{\text{old}}|}{|\tilde{\boldsymbol{\Sigma}}|} \leq \epsilon_{\boldsymbol{\Sigma}},$$

where d is the number of degrees of freedom (DoF). Once again, differentiating and solving the dual $g(\eta)$ for the projected covariance yields

$$\tilde{\boldsymbol{\Sigma}} = \left(\frac{\eta^* \boldsymbol{\Sigma}_{\text{old}}^{-1} + \boldsymbol{\Sigma}^{-1}}{\eta^* + 1} \right)^{-1} \quad \text{with} \quad \eta^* = \arg \min_{\eta} g(\eta), \quad \text{s.t.} \quad \eta \geq 0.$$

Here, the the optimal Lagrange multiplier η^* cannot be computed in closed form, however, a standard numerical optimizer, such as BFGS, is able to efficiently find it. This can be made differentiable by taking the differentials of the KKT conditions of the dual. For more details, we refer to the original work (Otto et al., 2021).

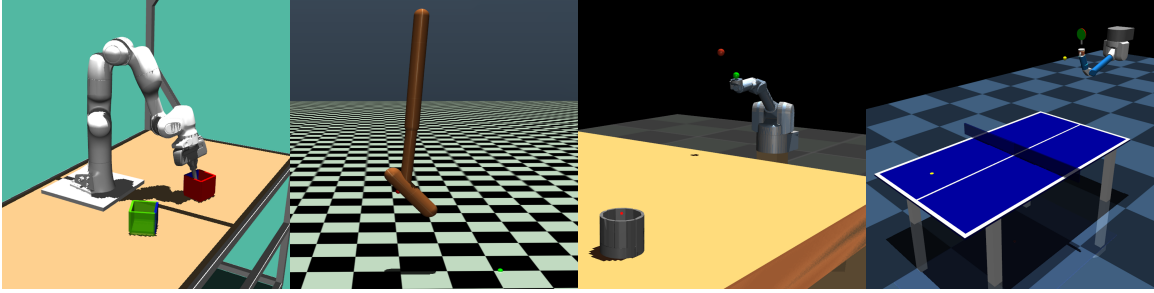


Figure 11: Visualization of the four control tasks box pushing, hopper jumping, beer pong, and table tennis.

Appendix C. Environment Details

C.1 Reacher5d

For the Reacher task we modify the original OpenAI gym Reacher-v2 by adding three additional joints, resulting in a total of five joints. The task goal is still to minimize the distance between the goal point \mathbf{p}_{goal} and the end-effector \mathbf{p} . We, however, only sample the goal point for $y \geq 0$, i. e. in the first two quadrants, to slightly reduce task complexity while maintaining the increased control complexity. The observation space remains unchanged, unless for the sparse reward where we additionally add the current step value to make learning possible for step-based methods. The context space only contains the coordinates of the goal position. The action space is the 5d equivalent to the original version.

For the reward the original setting leverages the goal distance

$$R_{goal} = \|\mathbf{p} - \mathbf{p}_{goal}\|_2$$

and the action cost

$$\tau_t = \sum_i^K (a_t^i)^2,$$

Dense Reward. The dense reward in the 5d setting, hence, stays the same and the agent receives in each time step t

$$R_{tot} = -\tau_t - R_{goal}$$

Sparse Reward. The sparse reward only returns the task reward in the last time step T and additionally adds a velocity penalty $R_{vel} = \sum_i^K (\dot{q}_T^i)^2$, where $\dot{\mathbf{q}}$ are the joint velocities, to avoid overshooting

$$R_{tot} = \begin{cases} -\tau_t & t < T, \\ -\tau_t - 200R_{goal} - 10R_{vel} & t = T. \end{cases}$$

C.2 Box Pushing

The goal of the box-pushing task is to move a box to a specified goal location and orientation using the seven DoF Franka Emika Panda. Hence, the context space for this task is the goal position $x \in [0.3, 0.6]$, $y \in [-0.45, 0.45]$ and the goal orientation $\theta \in [0, 2\pi]$. In addition to the contexts, the observation space for the step-based algorithms contains the positions and velocities of the joint angles, as well as position and orientation quaternions for the actual box and the target. For the action space we use the torques per joint and additionally add gravity compensation in each time step, that does not have to be learnt. The task is considered successfully solved if the position distance $\leq 0.05\text{m}$ and the orientation error $\leq 0.5\text{rad}$. For the total reward we consider different sub-rewards. First, the distance to the goal

$$R_{\text{goal}} = \|\mathbf{p} - \mathbf{p}_{\text{goal}}\|,$$

where \mathbf{p} is the box position and \mathbf{p}_{goal} the goal position itself. Second, the rotation distance

$$R_{\text{rotation}} = \frac{1}{\pi} \arccos |\mathbf{r} \cdot \mathbf{r}_{\text{goal}}|,$$

where \mathbf{r} and \mathbf{r}_{goal} are the box orientation and goal orientation in quaternion, respectively. Third, an incentive to keep the rod within the box

$$R_{\text{rod}} = \text{clip}(\|\mathbf{p} - \mathbf{h}_{\text{pos}}\|, 0.05, 10)$$

where \mathbf{h}_{pos} is the position of the rod tip. Fourth, a similar incentive that encourages to maintain the rod in a desired rotation

$$R_{\text{rod.rotation}} = \text{clip}\left(\frac{2}{\pi} \arccos |\mathbf{h}_{\text{rot}} \cdot \mathbf{h}_0|, 0.25, 2\right),$$

where \mathbf{h}_{rot} and $\mathbf{h}_0 = (0.0, 1.0, 0.0, 0.0)$ are the current and desired rod orientation in quaternion, respectively. And lastly, we utilize the following error

$$\text{err}(\mathbf{q}, \dot{\mathbf{q}}) = \sum_{i \in \{i \mid |q_i| > |q_i^b|\}} (|q_i| - |q_i^b|) + \sum_{j \in \{j \mid |\dot{q}_j| > |\dot{q}_j^b|\}} (|\dot{q}_j| - |\dot{q}_j^b|).$$

Here, \mathbf{q} , $\dot{\mathbf{q}}$, \mathbf{q}^b , and $\dot{\mathbf{q}}^b$ are the robot joint's position and velocity as well as their respective bounds. Additionally, we consider an action cost in each time step t

$$\tau_t = \sum_i^K (a_t^i)^2,$$

where $K = 7$ is the number of DoF. Similar to the aforementioned reacher task, we consider both dense and sparse reward setups.

Dense Reward. The dense reward provides information about the goal and rotation distance in each time step t on top of the utility rewards

$$R_{\text{tot}} = -R_{\text{rod}} - R_{\text{rod.rotation}} - 5e^{-4}\tau_t - \text{err}(\mathbf{q}, \dot{\mathbf{q}}) - 3.5R_{\text{goal}} - 2R_{\text{rotation}}.$$

Temporal Sparse Reward. The time-dependent sparse reward is similar to the dense reward, but only returns the goal and rotation distance in the last time step T

$$R_{\text{tot}} = \begin{cases} -R_{\text{rod}} - R_{\text{rod,rotation}} - 0.02\tau_t - \text{err}(\mathbf{q}, \dot{\mathbf{q}}), & t < T, \\ -R_{\text{rod}} - R_{\text{rod,rotation}} - 0.02\tau_t - \text{err}(\mathbf{q}, \dot{\mathbf{q}}) - 350R_{\text{goal}} - 200R_{\text{rotation}}, & t = T. \end{cases}$$

Goal Switching. To demonstrate the ability of our algorithm to handle the changing goal. We randomly switch to a new target at 20% of the max episode length. To ensure that the new target is solvable within the given episode length, we sample its position near to the old target position. The new target position, denoted as $[x_{\text{new}}, y_{\text{new}}]$, is computed as follows:

$$[x_{\text{new}}, y_{\text{new}}] = [x_{\text{old}}, y_{\text{old}}] + [\Delta x, \Delta y],$$

where $\Delta x, \Delta y$ are randomly sampled within the range $[-0.25, 0.2]$. Additionally, the new target orientation is determined by uniformly sampling a value from the range of $[0, 2\pi]$.

C.3 Hopper Jump

In the Hopper jump task the agent has to learn to jump as high as possible and land on a certain goal position at the same time. We consider five basis functions per joint resulting in an 15 dimensional weight space. The context is four-dimensional consisting of the initial joint angles $\theta \in [-0.5, 0]$, $\gamma \in [-0.2, 0]$, $\phi \in [0, 0.785]$ and the goal landing position $x \in [0.3, 1.35]$. The full observation space extends the original observation space from the OpenAI gym Hopper by adding the x-value of the goal position and the x-y-z difference between the goal point and the reference point at the Hopper’s foot. The action space is the same as for the original Hopper task. We consider a non-Markovian reward function for the episode-based algorithms and a step-based reward for PPO, which we have extensively designed to obtain the highest possible jump.

Non-Markovian Reward. In each time-step t we provide an action cost

$$\tau_t = 10^{-3} \sum_i^K (a_t^i)^2,$$

where $K = 3$ is the number of DoF. In the last time-step T of the episode we provide a reward which contains information about the whole episode as

$$\begin{aligned} R_{\text{height}} &= 10h_{\text{max}}, \\ R_{\text{gdist}} &= \|p_{\text{foot},T} - p_{\text{goal}}\|_2, \\ R_{\text{cdist}} &= \|p_{\text{foot,contact}} - p_{\text{goal}}\|_2, \\ R_{\text{healthy}} &= \begin{cases} 2 & \text{if } z_T \in [0.5, \infty] \text{ and } \theta, \gamma, \phi \in [-\infty, \infty] \\ 0 & \text{else} \end{cases}, \end{aligned}$$

where h_{max} is the maximum jump height in z-direction of the center of mass reached during the whole episode, $p_{\text{foot},t}$ is the x-y-z position of the foot’s heel at time step t , $p_{\text{foot,contact}}$ is the foot’s heel position when having a contact with the ground after the first jump, p_{goal} is the goal landing position of the heel. R_{healthy} is a slightly modified reward of the healthy

reward defined in the original hopper task. The hopper is considered as 'healthy' if the z position of the center of mass is within the range $[0.5m, \infty]$. This encourages the hopper to stand at the end of the episode. Note that all states need to be within the range $[-100, 100]$ for $R_{healthy}$. Since this is defined in the hopper task from OpenAI already, we haven't mentioned it here. The total reward at the end of an episode is given as

$$R_{tot} = - \sum_{t=0}^T \tau_t + R_{height} + R_{gdist} + R_{cdist} + R_{healthy}.$$

Step-Based Reward. We consider a step-based alternative reward such that PPO is also able to learn a meaningful behavior on this task. We have tuned the reward such that we can obtain the best performance. The observation space is the same as in the original hopper task from OpenAI extended with the goal landing position and the current distance of the foot's heel and the goal landing position. We again consider the action cost in each time-step t

$$\tau_t = 10^{-3} \sum_i^K (a_t^i)^2,$$

and additionally consider the rewards

$$\begin{aligned} R_{height,t} &= 3h_t \\ R_{gdist,t} &= 3\|p_{foot,t} - p_{goal}\|_2 \\ R_{healthy,t} &= \begin{cases} 1 & \text{if } z_t \in [0.5, \infty] \text{ and } \theta, \gamma, \phi \in [-\infty, \infty] \\ 0 & \text{else} \end{cases}, \end{aligned}$$

where these rewards are now returned to the agent in each time-step t , resulting in the reward per time-step

$$r_t(s_t, a_t) = -\tau_t + R_{height,t} + R_{gdist,t} + R_{healthy,t}.$$

C.4 Beer Pong

In the Beer Pong task the $K = 7$ Degrees of Freedom (DoF) robot has to throw a ball into a cup on a big table. The context is defined by the cup's two dimensional position on the table which lies in the range $x \in [-1.42, 1.42]$, $y \in [-4.05, -1.25]$. For the step-based algorithms we consider cosine and sine of the robot's joint angles, the angle velocities, the ball's distance to the bottom of the cup, the ball's distance to the top of the cup, the cup position and the current time step. The action space for the step-based algorithms is defined as the torques for each joint, the parameter space for the episode-based methods is 15 dimensional which consists of the two weights for the basis functions per joint and the duration of the throwing trajectory, i.e. the ball release time.

We generally consider action penalties

$$\tau_t = \frac{1}{K} \sum_i^K (a_t^i)^2,$$

consisting of the sum of squared torques per joint. For $t < T$ we consider the reward

$$r_t(s_t, a_t) = -\alpha_t \tau_t,$$

with $\alpha_t = 10^{-2}$. For $t = T$ we consider the non-Markovian reward

$$R_{task} = \begin{cases} -4 - \min(\|p_{c,top} - p_{b,1:T}\|_2^2) - 0.5\|p_{c,bottom} - p_{b,T}\|_2^2 \cdots \\ \cdots - 2\|p_{c,bottom} - p_{b,k}\|_2^2 - \alpha_T \tau, & \text{if cond. 1} \\ -4 - \min(\|p_{c,top} - p_{b,1:T}\|_2^2) - 0.5\|p_{c,bottom} - p_{b,T}\|_2^2 - \alpha_T \tau, & \text{if cond. 2} \\ -2 - \min(\|p_{c,top} - p_{b,1:T}\|_2^2) - 0.5\|p_{c,bottom} - p_{b,T}\|_2^2 - \alpha_T \tau, & \text{if cond. 3} \\ -\|p_{c,bottom} - p_{b,T}\|_2^2 - \alpha_T \tau, & \text{if cond. 4} \end{cases}$$

$$R_{task} = \begin{cases} -4 - \min(\|p_{c,top} - p_{b,1:T}\|_2^2) - 0.5\|p_{c,bottom} - p_{b,T}\|_2^2 \cdots \\ \cdots - 2\|p_{c,bottom} - p_{b,k}\|_2^2 - \alpha_T \tau, & \text{if cond. 1} \\ -4 - \min(\|p_{c,top} - p_{b,1:T}\|_2^2) - 0.5\|p_{c,bottom} - p_{b,T}\|_2^2 - \alpha_T \tau, & \text{if cond. 2} \\ -2 - \min(\|p_{c,top} - p_{b,1:T}\|_2^2) - 0.5\|p_{c,bottom} - p_{b,T}\|_2^2 - \alpha_T \tau, & \text{if cond. 3} \\ -\|p_{c,bottom} - p_{b,T}\|_2^2 - \alpha_T \tau, & \text{if cond. 4} \end{cases},$$

where $p_{c,top}$ is the position of the top edge of the cup, $p_{c,bottom}$ is the ground position of the cup, $p_{b,t}$ is the position of the ball at time point t , and τ is the squared mean torque over all joints during one rollout and $\alpha_T = 10^{-4}$. The different conditions are:

- cond. 1: The ball had a contact with the ground before having a contact with the table.
- cond. 2: The ball is not in the cup and had no table contact
- cond. 3: The ball is not in the cup and had table contact
- cond. 4: The ball is in the cup.

Note that $p_{b,k}$ is the ball's and the ground's contact position and is only given, if the ball had a contact with the ground first.

At time step $t = T$ we also give information whether the agent's chosen ball release time B was reasonable

$$R_{release} = \begin{cases} -30 - 10(B - B_{min})^2, & \text{if } B < B_{min} \\ -30 - 10(B - B_{max})^2, & \text{if } B < B_{max} \end{cases},$$

where we define $B_{min} = 0.1s$ and $B_{max} = 1s$, such that the agent is encouraged to throw the ball within the time range $[B_{min}, B_{max}]$.

The total return over the whole episode is therefore given as

$$R_{tot} = \sum_{t=1}^{T-1} r_t(s_t, a_t) + R_{task} + R_{release}$$

A throw is considered as successful if the ball is in the cup at the end of an episode.

C.5 Table Tennis

We consider table tennis for the entire table, i. e. incoming balls are anywhere on the side of the robot and goal locations anywhere on the opponents side. The goal is to use the 7 DoFs robotic arm to hit the incoming ball based on its landing position and return it as close as possible to the specified goal location. As context space we consider the initial ball position $x \in [-1, -0.2]$, $y \in [-0.65, 0.65]$ and the goal position $x \in [-1.2, -0.2]$, $y \in [-0.6, 0.6]$. The full observation space again contains the positions and velocities of the joints on top of the above context information. The torques of the joints make up the action space. For this experiment, we do not use any gravity compensation and allow in the episode-based setting to learn the start time t_0 and the trajectory duration T . The task is considered successful if the returned ball lands on the opponent’s side of the table and within $\leq 0.2\text{m}$ to the goal location. The max episode length of the table tennis environment is 350 steps. However, to accelerate the simulation, the episode will end immediately if any of the following terminated conditions are met:

- terminated cond. 1: A contact between the ball and the floor is detected,
- terminated cond. 2: The agent has hit the ball and then a contact between the ball and the table is detected.

The reward signal in the table tennis environment is defined as

$$r_{task} = \begin{cases} 0, & \text{if cond. 1} \\ 0.2 - 0.2 \tanh(\min \|\mathbf{p}_r - \mathbf{p}_b\|^2), & \text{if cond. 2} \\ 3 - 2 \tanh(\min \|\mathbf{p}_r - \mathbf{p}_b\|^2) - \tanh(\|\mathbf{p}_l - \mathbf{p}_{goal}\|^2), & \text{if cond. 3} \\ 6 - 2 \tanh(\min \|\mathbf{p}_r - \mathbf{p}_b\|^2) - 4 \tanh(\|\mathbf{p}_l - \mathbf{p}_{goal}\|^2), & \text{if cond. 4} \\ 7 - 2 \tanh(\min \|\mathbf{p}_r - \mathbf{p}_b\|^2) - 4 \tanh(\|\mathbf{p}_l - \mathbf{p}_{goal}\|^2), & \text{if cond. 5} \end{cases}$$

where \mathbf{p}_r is the position of racket center, \mathbf{p}_b is the position of the ball, \mathbf{p}_l is the ball landing position, \mathbf{p}_{goal} is the target position. The different conditions are

- cond. 1: the end of episode is not reached,
- cond. 2: the end of episode is reached,
- cond. 3: cond.2 is satisfied and robot did hit the ball,
- cond. 4: cond.3 is satisfied and the returned ball landed on the table,
- cond. 5: cond.4 is satisfied and the landing position is at the opponent’s side.

The episode ends when any of the following conditions are met

- the maximum horizon length is reached
- ball did land on the floor without hitting
- ball did land on the floor or table after hitting

For BBRL-PPO and BBRL-TRPL, the whole desired trajectory is obtained ahead of environment interaction, making use of this property we can collect some samples without physical simulation. The reward function based on this desired trajectory is defined as

$$r_{traj} = - \sum_{(i,j)} |\tau_{ij}^d| - |q_j^b|, \quad (i,j) \in \{(i,j) \mid |\tau_{ij}^d| > |q_j^b|\}$$

where τ^d is the desired trajectory, i is the time index, j is the joint index, q^b is the joint position upperbound. The desired trajectory is considered as invalid if $r_{traj} < 0$, an invalid trajectory will not be executed by robot. The overall reward for BBRL is defined as:

$$r = \begin{cases} r_{traj}, & r_{traj} < 0 \\ r_{task}, & \text{otherwise} \end{cases}$$

Goal Switching. To evaluate the capability of our approach in handling goal changes in the presence of non-Markovian reward, we designed a goal-switching task based on the table tennis environment. Given that the episode lengths are not fixed in this environment, we fixed the target changing time at the 99-th step after the episode begins. To simplify the task and make it easier to visualize, we restricted the range of the randomly sampled initial target to the left half of the table, specifically $y \in [-0.65, 0], x \in [-1.2, 0.2]$. At the 99-th step, there is 50% of chance that the goal is switched to another random position from the right side of the table, namely $y \in [0, 0.65], x \in [-1.2, 0.2]$.

Wind as External Perturbation. To further investigate the performance of our approach in handling environmental perturbations, we introduced artificial wind to the environment. At the beginning of each episode, we randomly sample a value $f \in [-0.1, 0.1]$ to represent the constant wind force. This force was then applied as an external force to the ball at each simulation step. It’s important to note that, in this specific task, we also augmented the observation space of the agent to include the velocity of the ball. By incorporating this information, the agent was able to infer the underlying ”wind speed” and adjust its behavior accordingly. Since this information is not directly observable at the beginning of the episode, episode-based policies, struggled to solve the task.

Appendix D. Additional Evaluations

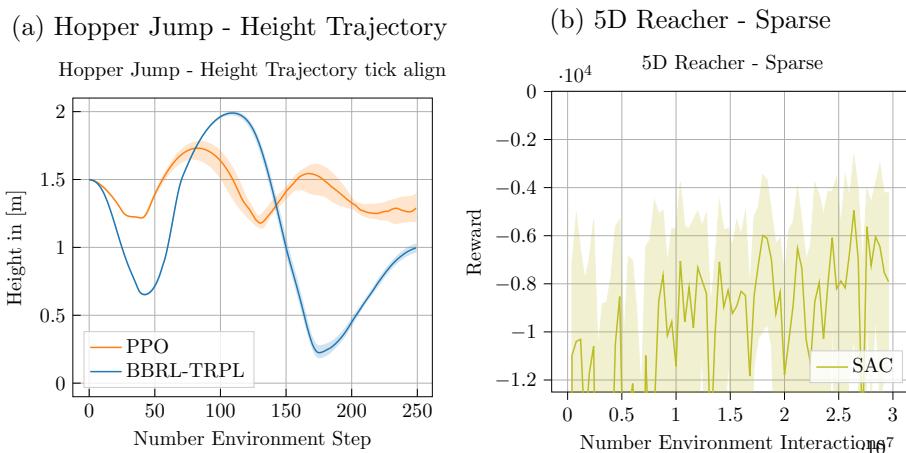


Figure 12: a The improved performance on the Hopper Jump task is also demonstrated on the jumping profile for a fixed context. While MP3-BB jumps once as high as possible, PPO constantly tries to maximize the height at each time step which leads to several jumps throughout the episode and consequently to a lower maximum height. b Learning curve of SAC for the sparse reward of the 5D Reacher task.

Appendix E. Hyperparameters

For all methods, where applicable, we optimized the learning rate, sample size, batch size, number of layers, and the number of epochs. For all MP based methods, we additionally optimized the number of basis functions. Moreover, we found that NDP requires tuning of the scale of the predicted DMP weights, which was hard-coded to 100 in the original code base. However, this value only worked for the Meta-World tasks, but not for the other tasks, hence we adjusted it to allow for a fair comparison. The population size of ES is always half the number of samples because two function evaluations are used per parameter vector.

Table 1: Hyperparameters for the 5D Reacher experiments.

	PPO	NDP	TRPL	SAC	CMORE	ES	MP3-BB-PPO	MP3-BB
number samples	16000	16000	16000	1000	120	200	64	64
GAE λ	0.95	0.95	0.95	0.95	n.a.	n.a.	n.a.	n.a.
discount factor	0.99	0.99	0.99	0.99	n.a.	n.a.	n.a.	n.a.
ϵ_μ/ϵ	n.a.	n.a.	0.005	n.a.	0.1	n.a.	n.a.	0.05
ϵ_Σ	n.a.	n.a.	0.0005	n.a.	n.a.	n.a.	n.a.	0.0005
optimizer	adam	adam	adam	adam	n.a.	adam	adam	adam
epochs	10	10	20	1000	n.a.	n.a.	100	100
learning rate	3e-4	3e-4	5e-5	3e-4	n.a.	1e-2	3e-4	3e-4
use critic	True	True	True	True	False	False	False	False
epochs critic	10	10	10	1000	n.a.	n.a.	n.a.	n.a.
learning rate critic (and alpha)	3e-4	3e-4	3e-4	3e-4	n.a.	n.a.	n.a.	n.a.
number minibatches	32	32	64	n.a.	n.a.	n.a.	1	1
batch size	n.a.	n.a.	n.a.	256	n.a.	n.a.	n.a.	n.a.
buffer size	n.a.	n.a.	n.a.	1e6	n.a.	n.a.	n.a.	n.a.
learning starts	0	0	0	10000	0	0	0	0
polyak_weight	n.a.	n.a.	n.a.	5e-3	n.a.	n.a.	n.a.	n.a.
trust region loss weight	n.a.	n.a.	10	n.a.	n.a.	n.a.	n.a.	10
normalized observations	True	True	True	False	False	False	False	False
normalized rewards	True	True	False	False	False	False	False	False
observation clip	10.0	10.0	n.a.	n.a.	n.a.	n.a.	n.a.	n.a.
reward clip	10.0	10.0	n.a.	n.a.	n.a.	n.a.	n.a.	n.a.
critic clip	0.2	0.2	n.a.	n.a.	n.a.	n.a.	0.2	n.a.
importance ratio clip	0.2	0.2	n.a.	n.a.	n.a.	n.a.	0.2	n.a.
hidden layers	[32, 32]	[32, 32]	[32, 32]	[128,128]	n.a.	[32, 32]	[32, 32]	[32, 32]
hidden layers critic	[32, 32]	[32, 32]	[32, 32]	[128,128]	n.a.	n.a.	n.a.	n.a.
hidden activation	tanh	tanh	tanh	relu	n.a.	tanh	tanh	tanh
initial std	1.0	1.0	1.0	1.0	1.0	1.0	1.0	1.0
number basis functions	n.a.	5	n.a.	n.a.	5	n.a.	5	5
number zero basis	n.a.	n.a.	n.a.	n.a.	1	n.a.	1	1
weight scale	n.a.	20	n.a.	n.a.	n.a.	n.a.	n.a.	n.a.

Table 2: Hyperparameters for the box pushing experiments.

	PPO	NDP	TRPL	SAC	ES	MP3	MP3-BB-PPO	MP3-BB
number samples	16000	16000	16000	1000	250	160	160	40
GAE λ	0.95	0.95	0.95	0.95	n.a.	n.a.	n.a.	n.a.
discount factor	1.0	0.99	1.0	0.99	n.a.	1.0	n.a.	n.a.
ϵ_μ	n.a.	n.a.	0.005	n.a.	n.a.	0.05	n.a.	0.05
ϵ_Σ	n.a.	n.a.	0.00005	n.a.	n.a.	0.0005	n.a.	0.0005
optimizer	adam	adam	adam	adam	adam	adam	adam	adam
epochs	10	10	20	1000	n.a.	20	100	20
learning rate	1e-4	1e-4	5e-5	1e-4	1e-2	3e-4	1e-4	3e-4
use critic	True	True	True	True	False	True	True	True
epochs critic	10	10	10	1000	n.a.	10	100	10
learning rate critic (and alpha)	1e-4	1e-4	2e-4	1e-4	n.a.	3e-4	1e-4	3e-4
number minibatches	40	32	40	n.a.	n.a.	1	1	1
batch size	n.a.	n.a.	n.a.	256	n.a.	n.a.	n.a.	n.a.
buffer size	n.a.	n.a.	n.a.	1e6	n.a.	n.a.	n.a.	n.a.
learning starts	0	0	0	10000	0	0	0	0
polyak_weight	n.a.	n.a.	n.a.	5e-3	n.a.	n.a.	n.a.	n.a.
trust region loss weight	n.a.	n.a.	10	n.a.	n.a.	10	n.a.	10
normalized observations	True	True	True	False	False	False	False	False
normalized rewards	True	True	False	False	False	False	False	False
observation clip	10.0	10.0	n.a.	n.a.	n.a.	n.a.	n.a.	n.a.
reward clip	10.0	10.0	n.a.	n.a.	n.a.	n.a.	n.a.	n.a.
critic clip	0.2	0.2	n.a.	n.a.	n.a.	n.a.	0.2	n.a.
importance ratio clip	0.2	0.2	n.a.	n.a.	n.a.	n.a.	0.2	n.a.
hidden layers	[256, 256]	[256, 256]	[256, 256]	[256, 256]	[256, 256]	[128, 128]	[128, 128]	[128, 128]
hidden layers critic	[256, 256]	[256, 256]	[256, 256]	[256, 256]	n.a.	[32, 32]	[32, 32]	[32, 32]
hidden activation	tanh	tanh	tanh	relu	tanh	relu	tanh	relu
initial std	1.0	1.0	1.0	1.0	1.0	1.0	1.0	1.0
MP type	n.a.	DMP	n.a.	n.a.	n.a.	ProDMP	ProMP	ProMP
number basis functions	n.a.	5	n.a.	n.a.	n.a.	4	5	5
number zero basis	n.a.	n.a.	n.a.	n.a.	n.a.	0	1	1
k	n.a.	5	n.a.	n.a.	n.a.	25	100	100
weight scale	n.a.	10	n.a.	n.a.	n.a.	n.a.	n.a.	n.a.

Table 3: Hyperparameters for the Meta-World experiments.

	PPO	NDP	TRPL	SAC	ES	MP3	MP3-BB-PPO	MP3-BB
number samples	16000	16000	16000	1000	200	64	16	16
GAE λ	0.95	0.95	0.95	0.95	n.a.	1	n.a.	n.a.
discount factor	0.99	0.99	0.99	0.99	n.a.	1	n.a.	n.a.
ϵ_μ	n.a.	n.a.	0.005	n.a.	n.a.	0.075	n.a.	0.005
ϵ_Σ	n.a.	n.a.	0.0005	n.a.	n.a.	0.0005	n.a.	0.0005
optimizer	adam	adam	adam	adam	adam	adam	adam	adam
epochs	10	10	20	1000	n.a.	10	100	100
learning rate	3e-4	3e-4	5e-5	3e-4	1e-2	5e-5	3e-4	3e-4
use critic	True	True	True	True	False	True	False	False
epochs critic	10	10	10	1000	n.a.	10	n.a.	n.a.
learning rate critic (and alpha)	3e-4	3e-4	3e-4	3e-4	n.a.	3e-4	n.a.	n.a.
number minibatches	32	32	64	n.a.	n.a.	32	1	1
batch size	n.a.	n.a.	n.a.	256	n.a.	n.a.	n.a.	n.a.
buffer size	n.a.	n.a.	n.a.	1e6	n.a.	n.a.	n.a.	n.a.
learning starts	0	0	0	10000	0	0	0	0
polyak_weight	n.a.	n.a.	n.a.	5e-3	n.a.	n.a.	n.a.	n.a.
trust region loss weight	n.a.	n.a.	10	n.a.	n.a.	10	n.a.	10
normalized observations	True	True	True	False	False	True	False	False
normalized rewards	True	True	False	False	False	False	False	False
observation clip	10.0	10.0	n.a.	n.a.	n.a.	n.a.	n.a.	n.a.
reward clip	10.0	10.0	n.a.	n.a.	n.a.	n.a.	n.a.	n.a.
critic clip	0.2	0.2	n.a.	n.a.	n.a.	n.a.	0.2	n.a.
importance ratio clip	0.2	0.2	n.a.	n.a.	n.a.	n.a.	0.2	n.a.
hidden layers	[128, 128]	[128, 128]	[128, 128]	[256, 256]	[128, 128]	[256, 256]	[32, 32]	[32, 32]
hidden layers critic	[128, 128]	[128, 128]	[128, 128]	[256, 256]	n.a.	[256, 256]	n.a.	n.a.
hidden activation	tanh	tanh	tanh	relu	tanh	tanh	tanh	relu
initial std	1.0	1.0	1.0	1.0	1.0	1.0	1.0	1.0
MP type	n.a.	DMP	n.a.	n.a.	n.a.	ProDMP	ProMP	ProMP
number basis functions	n.a.	5	n.a.	n.a.	n.a.	3	5	5
number zero basis	n.a.	n.a.	n.a.	n.a.	n.a.	n.a.	1	1
k	n.a.	n.a.	n.a.	n.a.	n.a.	100	n.a.	n.a.
weight scale	n.a.	100	n.a.	n.a.	n.a.	10	10	10

Table 4: Hyperparameters for the Hopper Jump experiments.

	PPO	TRPL	SAC	CMORE	ES	MP3-BB-PPO	MP3-BB
number samples	16384	16384	1000	60	200	64	64
GAE λ	0.95	0.95	0.95	n.a.	n.a.	n.a.	n.a.
discount factor	0.99	0.99	0.99	n.a.	n.a.	n.a.	n.a.
ϵ_μ/ϵ	n.a.	0.005	n.a.	0.1	n.a.	n.a.	0.005
ϵ_Σ	n.a.	0.00005	n.a.	n.a.	n.a.	n.a.	0.0005
optimizer	adam	adam	adam	n.a.	adam	adam	adam
epochs	10	20	1000	n.a.	n.a.	100	100
learning rate	3e-4	5e-5	1e-4	n.a.	0.01	1e-4	5e-5
use critic	True	True	True	False	False	False	False
epochs critic	10	10	1000	n.a.	n.a.	n.a.	n.a.
learning rate critic (and alpha)	3e-4	3e-4	1e-4	n.a.	n.a.	n.a.	n.a.
number minibatches	32	64	n.a.	n.a.	n.a.	1	1
batch size	n.a.	n.a.	256	n.a.	n.a.	n.a.	n.a.
buffer size	n.a.	n.a.	1e6	n.a.	n.a.	n.a.	n.a.
learning starts	0	0	10000	0	0	0	0
polyak_weight	n.a.	n.a.	5e-3	n.a.	n.a.	n.a.	n.a.
trust region loss weight	n.a.	10	n.a.	n.a.	n.a.	n.a.	25
normalized observations	True	True	False	False	False	False	False
normalized rewards	True	False	False	False	False	False	False
observation clip	10.0	n.a.	n.a.	n.a.	n.a.	n.a.	n.a.
reward clip	10.0	n.a.	n.a.	n.a.	n.a.	n.a.	n.a.
critic clip	0.2	n.a.	n.a.	n.a.	n.a.	0.2	n.a.
importance ratio clip	0.2	n.a.	n.a.	n.a.	n.a.	0.2	n.a.
hidden layers	[128, 128]	[128, 128]	[128, 128]	n.a	[128, 128]	[32, 32]	[32, 32]
hidden layers critic	[128, 128]	[128, 128]	[128, 128]	n.a	n.a	n.a	n.a
hidden activation	tanh	tanh	relu	n.a.	tanh	tanh	tanh
initial std	1.0	1.0	1.0	1.0	1.0	1.0	1.0
number basis functions	n.a.	n.a.	n.a.	5	n.a.	5	5
number zero basis	n.a.	n.a.	n.a.	1	n.a.	1	1

Table 5: Hyperparameters for the Beer Pong experiments.

	PPO	CMORE	BBRL-PPO	BBRL-TRPL
number samples	16384	60	160	160
GAE λ	0.95	n.a.	n.a.	n.a.
discount factor	0.99	n.a.	n.a.	n.a.
ϵ_μ/ϵ	n.a.	0.1	n.a.	0.005
ϵ_Σ	n.a.	n.a.	n.a.	0.0005
optimizer	adam	n.a.	adam	adam
epochs	10	n.a.	100	100
learning rate	3e-4	n.a.	1e-4	5e-5
use critic	True	False	False	False
epochs critic	10	n.a.	n.a.	n.a.
learning rate critic (and alpha)	3e-4	n.a.	n.a.	n.a.
number minibatches	32	n.a.	1	1
trust region loss weight	n.a.	n.a.	n.a.	25
normalized observations	True	False	False	False
normalized rewards	True	False	False	False
observation clip	10.0	n.a.	n.a.	n.a.
reward clip	10.0	n.a.	n.a.	n.a.
critic clip	0.2	n.a.	0.2	n.a.
importance ratio clip	0.2	n.a.	0.2	n.a.
hidden layers	[128, 128]	n.a.	[32, 32]	[32, 32]
hidden layers critic	[128, 128]	n.a.	n.a.	n.a.
hidden activation	tanh	n.a.	tanh	tanh
initial std	1.0	1.0	1.0	1.0
number basis functions	n.a.	2	2	2
number zero basis	n.a.	2	2	2

Table 6: Hyperparameters for the Table Tennis experiments.

	PPO	TRPL	MP3	BBRL-PPO	BBRL-TRPL
number samples	16000	16000	360	200	200
GAE λ	0.95	0.95	n.a.	n.a.	n.a.
discount factor	0.99	0.99	1.0	n.a.	n.a.
ϵ_μ	n.a.	0.0005	0.005	n.a.	0.0005
ϵ_Σ	n.a.	0.00005	0.0005	n.a.	0.00005
optimizer	adam	adam	adam	adam	adam
epochs	10	20	20	100	100
learning rate	1e-4	5e-5	2e-4	1e-4	3e-4
use critic	True	True	True	True	True
epochs critic	10	10	10	100	100
learning rate critic (and alpha)	1e-4	1e-4	2e-4	1e-4	3e-4
number minibatches	40	40	1	1	1
trust region loss weight	n.a.	10.0	10	n.a.	25
normalized observations	True	True	False	False	False
normalized rewards	True	False	False	False	False
observation clip	10.0	n.a.	n.a.	n.a.	n.a.
reward clip	10.0	n.a.	n.a.	n.a.	n.a.
critic clip	0.2	n.a.	n.a.	0.2	n.a.
importance ratio clip	0.2	n.a.	n.a.	0.2	n.a.
hidden layers	[256, 256]	[256, 256]	[256]	[256]	[256]
hidden layers critic	[256, 256]	[256, 256]	[256]	[256]	[256]
hidden activation	tanh	tanh	relu	tanh	relu
initial std	1.0	1.0	1.0	1.0	1.0
MP type	n.a.	n.a.	ProDMP	ProMP	ProMP
number basis functions	n.a.	n.a.	3	3	3
number zero basis	n.a.	n.a.	0	1	1
k	n.a.	n.a.	50	n.a.	n.a.
weight scale	n.a.	n.a.	n.a.	n.a.	n.a.